

A concept of polymeric networks with sliding junctions for the time-dependent response of filled elastomers

Aleksey D. Drozdov and Al Dorfmann
Institute of Structural Engineering
82 Peter Jordan Street
A-1190 Vienna, Austria

Abstract

Constitutive equations are derived for the time-dependent behavior of particle-reinforced elastomers at isothermal loading with finite strains. A rubbery polymer is modelled as a network of macromolecules bridged by junctions, where the junctions can slip with respect to the bulk material under straining. A filled rubbery compound is thought of as an ensemble of meso-regions where sliding occurs with different rates. Stress-strain relations for a particle-reinforced rubber are developed by using the laws of thermodynamics. For uniaxial tensile relaxation tests, these equations are determined by three adjustable parameters. To find the experimental constants, three series of tests are performed at longitudinal strains in the range from 100 to 250 %. By fitting observations, the effects of pre-loading and thermal recovery are analyzed on the nonlinear viscoelastic response of natural rubber reinforced with carbon black.

Key-words: Filled elastomers, Polymeric networks, Nonlinear viscoelasticity, Finite strains, Relaxation tests

1 Introduction

This paper is concerned with modelling the time-dependent behavior of particle-reinforced elastomers at isothermal loading with finite strains. The viscoelastic and viscoplastic responses of filled rubbers have been a focus of attention in the past decade, which may be explained by numerous applications of rubber-like materials in industry (vehicle tires, shock absorbers, earthquake bearings, seals, flexible joints, solid propellants, etc.), see, e.g., Govendjee and Simo (1992), Johnson and Stacer (1993), Häusler and Sayir (1995), Johnson et al. (1995), Aksel and Hübner (1996), Holzapfel and Simo (1996), Lion (1996, 1997, 1998), Spathis (1997), Bergström and Boyce (1998), Ha and Schapery (1998), Kaliske and Rothert (1998), Reese and Govindjee (1998), Septanika and Ernst (1998), Miehe and Keck (2000), Wu and Liechti (2000), Haupt and Sedlan (2001), to mention a few. Although the number of publications on this subject is rather large, some important issues remain, however, obscure.

One of the main questions to be resolved deals with the physical nature of the time-dependent response of rubber-like materials. It is worth noting that there is no agreement in the literature about the micro-mechanisms for stress relaxation in unfilled elastomers.

The viscoelastic behavior of rubbery polymers is conventionally modelled within the concept of temporary networks (Green and Tobolsky, 1946). A polymer is treated as a network of macromolecules bridged by junctions (chemical and physical cross-links, entanglements and inter-chain links induced by van der Waals forces). With reference to the affinity hypothesis, junctions are assumed to be rigidly connected with the bulk medium, whereas the time-dependent response is associated with breakage of active strands (whose ends are linked to separate junctions) and reformation of dangling strands (where stresses totally relax before these chains merge with the network).

Another scenario for stress relaxation in rubbery polymers is based on the concept of non-affine junctions that presumes the network of macromolecules to be permanent and explains the time-dependent response at the macro-level by slippage of junctions with respect to the bulk material at the micro-level. This approach was first suggested by Phan-Thien and Tanner (1977) and Phan-Thien (1978) for polymer melts and was applied by Desmorat and Cantournet (2001) to study the behavior of filled elastomers.

A version of the concept of non-affine networks, where junctions do not slide, but polymeric chains are allowed to slip with respect to entanglements was proposed by Miehe and co-authors for the analysis of stresses in rubbery vulcanizates (Miehe, 1995; Miehe and Keck, 2000, Lulei and Miehe, 2001). A similar model (where chains slip with respect to filler particles instead of entanglements) was recently introduced by Hansen (2000) with reference to results of molecular dynamics simulations and atomic force microscopy measurements.

The above theories concentrate on relatively slow relaxation processes when stresses relax at the time-scale of structural rearrangement in the entire macromolecule. A relatively fast relaxation process (whose characteristic time is associated with the time for rearrangement of a mechanical segment in a chain) was studied by Drozdov (2001) by using a micro-mechanical scenario for the time-dependent response of rubbery polymers similar to the tube model for concentrated polymeric solutions and melts (Doi and Edwards, 1986). The difference between the two approaches is that the conventional tube

theory is based on the reptation concept for polymeric chains (this kind of diffusive motion is prevented by cross-links in rubbery vulcanizates), whereas the concept of wavy tubes ascribes the viscoelastic behavior of rubbers at the macro-level to mechanically induced changes in the concentration of regions with high molecular mobility in an individual strand at the micro-level. A transition mechanism from relaxation processes at the length-scale of a statistical segment to those at the length-scale of a chain in a polymer melt was recently discussed by Herman (2001).

This brief discussion of basic concepts in finite viscoelasticity and viscoplasticity of rubber-like materials demonstrates that our knowledge of micro-mechanisms for the time-dependent response of unfilled elastomers is far away from being exhausted. The physics of the viscoelastic and viscoplastic behavior of particle-reinforced rubbers remains rather unclear. This conclusion is confirmed by a number of micro-mechanical theories that have been proposed in the past decade to describe the viscoelastic response of filled elastomers.

On the one hand, Aksel and Hübner (1996), Kaliske and Rothert (1998) and Hansen (2000) explained the time-dependent behavior of particle-reinforced rubbers by sliding of polymeric chains along and their de-wetting from the surfaces of filler clusters. This concept goes back to the model proposed by Dannenberg (1975), which, in turn, is equivalent to the neglect of the ability of a host matrix to relax, the hypothesis suggested about half a century ago by Bueche (1960, 1961) to explain the Mullins effect.

On the other hand, Liang et al. (1999), Clarke et al. (2000) and Leblanc and Cartault (2001) evidenced that the effect of particles and their aggregates on the viscoelastic response of rubbery compounds is not crucial. Leblanc and Cartault (2001) performed dynamic shear tests on uncured styrene-butadiene rubber reinforced with various amounts of carbon black and silica and reported rather limited time-dependent responses of the compounds. These observations allowed them to infer that inter-molecular interactions play the key role in the viscoelastic behavior, whereas the influence of filler is of second importance. Liang et al. (1999) reported experimental data in dynamic tensile tests on ternary composite of polypropylene and EPDM (ethylene propylene diene monomers) elastomer filled with glass beads. They demonstrated that treatment of beads by silane coupling agent did not affect mechanical damping and that the loss modulus of the compound with untreated beads decreased with the concentration of filler (in contrast with the de-wetting concept). Clarke et al. (2000) carried out tensile relaxation tests on two elastomers (natural polyisoprene rubber and synthetic polyacrylate rubber) and revealed significant relaxation of stresses in the unfilled natural rubber.

Our experimental data in tensile relaxation tests on natural rubber reinforced with high abrasion furnace black demonstrated comparable decreases in the longitudinal stress for a filled [45 phr (parts per hundred parts of rubber) of carbon black (CB)] and an unfilled [1 phr of CB] compounds (Drozdov and Dorfmann, 2001). Because the amount of stress relaxed during 1 hour at room temperature in the filled specimens exceeded that for the unfilled samples (approximately by twice), we conclude that a micro-mechanism for the viscoelastic response of filled elastomers is in between the above two extreme concepts: the relaxation process in particle-reinforced rubbers may be associated with rearrangement of macromolecules in the matrix, but the rearrangement process is strongly affected by local inhomogeneities induced by the presence of filler.

In accord with this picture, we model a filled rubber as a network of macromolecules

bridged by junctions. To account for the effect of filler particles and their agglomerates on the time-dependent response of the network in a tractable way, the network is treated as an ensemble of meso-domains, where rearrangement of strands occurs with different (mutually independent) rates. The characteristic size of these regions (roughly estimated as several hundreds of nm) is assumed to substantially exceed the radius of gyration for macromolecules and the average radius of particles, on the one hand, and to be noticeably less than the dimensions of a macro-specimen. The ensemble of meso-domains reflects local inhomogeneities in the rubber-like material caused by impurities, non-homogeneity in the spatial distribution of a cross-linker and a filler, segregation of short chains to interfaces between the filler clusters and the host matrix (Carlier et al., 2001), local fluctuations of elastic moduli associated with the presence of hard cores around filler particles and their clusters, as well as the enhancement of the rearrangement process for strands in the close vicinities of the filler aggregates (Karasek and Sumita, 1996). The work is confined to filled rubbers with the volume fractions of particles, φ , below the percolation threshold, which implies that phenomena associated with aggregation of clusters into an infinite secondary network (Yatsuyanagi et al., 2001) are not taken into account.

With reference to the concept of sliding junctions, different meso-regions are characterized by different potential energies, ω , for slippage of junctions with respect to the bulk material. The rate of slippage, Γ , is expressed in terms of the potential energy, ω , by the Boltzmann formula. This implies that the sliding process is entirely determined by the attempt rate, Γ_0 , and the distribution function, $p(\omega)$, of potential energies for sliding.

To account for the influence of strain intensity on the rate of stress relaxation, we distinguish between active meso-domains, where junctions can freely slide, and passive meso-regions, where sliding is prevented by surrounding macromolecules (because local concentrations of cross-links and van der Waals links between strands in these domains exceed their average values). Under stretching, some van der Waals links between strands break in passive meso-domains, which implies that these regions become active. The ability of a passive meso-region to be activated is determined by a measure of damage, α , that determines the relative number of extra links between macromolecules which do not permit the sliding process to start. The present study focuses on loading programs in which passive meso-regions are transformed into the active state when the stress intensity grows. Healing of inter-chain links that results in the inverse transformation at unloading is beyond the scope of this paper.

The objective of this paper is three-fold:

1. To develop constitutive equations for the time-dependent response of a particle-reinforced elastomer modelled as an ensemble of meso-regions with various potential energies for sliding of junctions.
2. To report experimental data in three series of tensile relaxation tests on CB filled natural rubber at various longitudinal strains in the range from 100 to 250 %. The first series of tests was carried out on virgin specimens, in the second series the samples were initially pre-loaded, whereas the third series dealt with the same specimens after thermal recovery at an elevated temperature.

3. To find adjustable parameters in the stress–strain relations by fitting observations and to rationalize the influence of pre-loading and thermal recovery on the nonlinear viscoelastic behavior of filled elastomers in terms of the constitutive model.

The study is organized as follows. Sliding of junctions in active meso-regions and transition of passive meso-domains into the active state are discussed in Section 2. Kinematic equations for slippage of junctions with respect to the bulk medium are developed in Section 3. The mechanical energy of a particle-reinforced elastomer is determined in Section 4. Stress–strain relations are derived in Section 5 by using the laws of thermodynamics. Uniaxial extension of a specimen is analyzed in Section 6. Section 7 deals with the description of the experimental procedure. Adjustable parameters in the constitutive equations are determined by fitting observations in Section 8, where a physical interpretation is provided for the findings. Some concluding remarks are formulated in Section 9.

2 Deformation of a filled elastomer

A particle-reinforced elastomer is modelled as an ensemble of meso-domains (with arbitrary shapes) where junctions can slip with respect to the bulk material. Sliding of junctions is assumed to occur independently in different meso-regions.

A meso-domain is characterized by its potential energy ω , which is defined as follows. Slippage of junctions with respect to their positions in the bulk material is thought of as a viscous flow with the constitutive equation

$$\sigma = \eta \dot{\epsilon}, \quad (1)$$

where σ is the stress, $\dot{\epsilon}$ is the strain rate, and $\eta > 0$ is some viscosity. The parameter η in Eq. (1) is given by

$$\eta = \frac{G}{\Gamma}, \quad (2)$$

where G stands for an elastic modulus, and Γ is the rate of sliding. For definiteness, we suppose that G coincides for all meso-domains, whereas Γ accepts different values for different regions. The Boltzmann formula is adopted for the rate of sliding

$$\Gamma = \Gamma_0 \exp\left(-\frac{\bar{\omega}}{k_B T}\right), \quad (3)$$

where $\bar{\omega}$ is the potential energy of a meso-region, T is the absolute temperature, k_B is Boltzmann's constant, and the pre-factor Γ_0 weakly depends on temperature. The attempt rate Γ_0 equals the rate of sliding for junctions at an elevated temperature ($T \rightarrow \infty$). Introducing the dimensionless potential energy,

$$\omega = \frac{\bar{\omega}}{k_B T_0},$$

where T_0 is some reference temperature, and disregarding the effect of small temperature increments, $\Delta T = T - T_0$, on the sliding process, we find from Eq. (3) that

$$\Gamma = \Gamma_0 \exp(-\omega). \quad (4)$$

Equation (4) expresses the rate of slippage of junctions with respect to the bulk medium, Γ , in a meso-region in terms of its potential energy, ω .

The potential energy ω characterizes the rate of sliding of junctions in a meso-domain where the sliding process is not affected by inter-chain interactions. The neglect of interaction between polymeric chains is a conventional hypothesis in the entropic theory of rubber elasticity (Treloar, 1975), where the number of available configurations for a chain is determined under the assumption that surrounding macromolecules do not restrict the chain geometry. For a filled elastomer, interactions between polymeric chains may be disregarded only for a part of the ensemble of meso-domains. In the other part of meso-regions these interactions prevent sliding of junctions until micro-strains become sufficiently large to break inter-chain links (these links reflect van der Waals' forces between strands) that do not allow the sliding process to start.

With reference to this picture, two groups of meso-domains in an ensemble are distinguished:

1. active regions where sliding of junctions is unrestricted,
2. passive domains where slippage of junctions is inhibited by inter-chain interactions.

The sliding process in an active meso-region is entirely determined by the potential energy, ω , of this domain. To characterize the ability of a passive meso-domain to become active, we introduce an additional variable, α , which is thought of as a measure for mechanically induced damage of inter-chain interactions.

Any interaction between polymeric chains that prevents slippage of junctions with respect to the bulk material may be thought of as a temporary link between macromolecules. The weakening of interaction between strands driven by mechanical factors is modelled as rupture of temporary links under loading.

Assuming the number of meso-regions with potential energy ω per unit mass of an elastomer to be rather large, we denote by $\langle M(\omega) \rangle$ the average number of inter-chain links per unit domain before loading, and by $M(t, \omega)$ the number of these links in a meso-domain in the deformed state at time t (the instant $t = 0$ corresponds to the time when external forces are applied to a specimen). The measure of damage, α , is defined as the ratio of these quantities,

$$\alpha(t, \omega) = \frac{M(t, \omega)}{\langle M(\omega) \rangle}. \quad (5)$$

Unlike conventional approaches to fracture of elastomers, where the initial measure of damage is assumed to vanish, whereas fracture of a macro-sample is associated with some positive value of the damage variable (conventionally, unity), Eq. (5) implies that α is non-negative in the stress-free state, and it decays to zero when a passive meso-region is transformed into an active one.

It follows from Eq. (5) that the initial value of the damage variable, α , may be either higher or lower than 1 in passive meso-domains, whereas the average value of $\alpha(0, \omega)$ equals unity. The condition $\alpha(0, \omega) < 1$ means that a passive meso-domain is initially damaged. This damage is associated with breakage of inter-chain interactions in meso-regions during the preparation process (at the stage of milling of a rubbery compound). On the other hand, the inequality $\alpha(0, \omega) > 1$ implies that the number of links between

macromolecules in a passive meso-domain in a virgin specimen exceeds its average value, which may be ascribed to local inhomogeneities in the distribution of a cross-linker.

In accord with this picture, the distribution of passive meso-domains is described by the function $\Xi_p(t, \alpha, \omega)$ that equals the current number of passive meso-regions (per unit mass) with the potential energy ω where the damage variable equals α . Summing the number of meso-domains with various measures of damage, α , we find the concentration of passive regions with potential energy ω ,

$$X_p(t, \omega) = \int_0^\infty \Xi_p(t, \alpha, \omega) d\alpha. \quad (6)$$

The number of passive domains per unit mass of an elastomer, N_p , equals the sum of the numbers of passive meso-regions with various potential energies, ω ,

$$N_p(t) = \int_0^\infty X_p(t, \omega) d\omega. \quad (7)$$

Denote by $X_a(t, \omega)$ the current number of active meso-domains with potential energy ω . The quantities X_a and X_p are connected by the conservation law

$$X_a(t, \omega) + X_p(t, \omega) = X(\omega), \quad (8)$$

where $X(\omega)$ is the concentration of meso-regions with potential energy ω . Differentiation of Eq. (8) with respect to time implies that

$$\gamma(t, \omega) = \frac{\partial X_a}{\partial t}(t, \omega) = -\frac{\partial X_p}{\partial t}(t, \omega), \quad (9)$$

where $\gamma(t, \omega)$ is the rate of transformation of passive meso-domains into active ones. Integrating Eq. (8) over ω and using Eq. (7), we find that

$$N_a(t) + N_p(t) = N, \quad (10)$$

where

$$N_a(t) = \int_0^\infty X_a(t, \omega) d\omega \quad (11)$$

is the current concentration of active meso-domains and

$$N = \int_0^\infty X(\omega) d\omega$$

is the total number of meso-regions per unit mass.

3 Kinematic relations

Let \mathbf{r}_0 be the radius vector of an arbitrary junction in the reference state, $\mathbf{r}(t, \mathbf{r}_0)$ its radius vector in the deformed state at time t , and $\mathbf{r}_u(t, \mathbf{r}_0)$ the radius vector of this point in the unloaded state. In what follows, the argument \mathbf{r}_0 of the functions \mathbf{r} and \mathbf{r}_u is omitted for the sake of simplicity.

The unloaded state of a meso-region characterizes changes in the positions of junctions at time t driven of their slippage with respect to the bulk material (i.e., by slippage with respect to the initial configuration of a specimen). The displacement vector for transition of a junction from its reference state to the unloaded state is given by

$$\mathbf{u}_u(t) = \mathbf{r}_u(t) - \mathbf{r}_0.$$

Denote by $\nabla_0 \mathbf{r}(t)$ the deformation gradient for transition from the reference state to the actual state, by $\nabla_0 \mathbf{r}_u(t)$ the deformation gradient for transition from the reference state to the unloaded state, and by $\nabla_u(t) \mathbf{r}(t)$ the deformation gradient for transition from the unloaded state to the deformed state. Here ∇_0 and $\nabla_u(t)$ are the gradient operators in the initial and unloaded configurations, respectively. With reference to Drozdov (1996), the “left” gradient operators are employed: the image, $d\mathbf{r}(t)$, in the actual state of an infinitesimal vector, $d\mathbf{r}_0$, in the reference state reads

$$d\mathbf{r}(t) = d\mathbf{r}_0 \cdot \nabla_0 \mathbf{r}(t),$$

where the dot stands for inner product. The deformation gradients are connected by the equation

$$\nabla_0 \mathbf{r}(t) = \nabla_0 \mathbf{r}_u(t) \cdot \nabla_u(t) \mathbf{r}(t), \quad (12)$$

which expresses the chain rule for differentiation of the vector function $\mathbf{r} = \mathbf{r}(t, \mathbf{r}_0)$ with respect to \mathbf{r}_0 .

The right Cauchy deformation tensor, $\mathbf{C}(t)$, for transition from the initial state to the deformed state is determined by the formula

$$\mathbf{C}(t) = \nabla_0 \mathbf{r}(t) \cdot [\nabla_0 \mathbf{r}(t)]^\top, \quad (13)$$

where \top denotes transpose. By analogy with Eq. (13), we introduce the right Cauchy deformation tensor for transition from the reference state to the unloaded state,

$$\mathbf{C}_u(t) = \nabla_0 \mathbf{r}_u(t) \cdot [\nabla_0 \mathbf{r}_u(t)]^\top, \quad (14)$$

and the right Cauchy deformation tensor for transition from the unloaded state to the actual state,

$$\mathbf{C}_e(t) = \nabla_u(t) \mathbf{r}(t) \cdot [\nabla_u(t) \mathbf{r}(t)]^\top. \quad (15)$$

It follows from Eqs. (12), (13) and (15) that

$$\begin{aligned} \mathbf{C}_e(t) &= [\nabla_0 \mathbf{r}_u(t)]^{-1} \cdot \nabla_0 \mathbf{r}(t) \cdot [\nabla_0 \mathbf{r}(t)]^\top \cdot [\nabla_0 \mathbf{r}_u(t)]^{-\top} \\ &= [\nabla_0 \mathbf{r}_u(t)]^{-1} \cdot \mathbf{C}(t) \cdot [\nabla_0 \mathbf{r}_u(t)]^{-\top}. \end{aligned} \quad (16)$$

The left Cauchy deformation tensor for transition from the reference state to the deformed state reads

$$\mathbf{B}(t) = [\nabla_0 \mathbf{r}(t)]^\top \cdot \nabla_0 \mathbf{r}(t), \quad (17)$$

whereas the left Cauchy deformation tensor for transition from the unloaded state to the actual state is given by

$$\mathbf{B}_e(t) = [\nabla_u(t)\mathbf{r}(t)]^\top \cdot \nabla_u(t)\mathbf{r}(t). \quad (18)$$

Equations (12), (14) and (18) imply that

$$\begin{aligned} \mathbf{B}_e(t) &= [\nabla_0\mathbf{r}(t)]^\top \cdot [\nabla_0\mathbf{r}_u(t)]^{-\top} \cdot [\nabla_0\mathbf{r}_u(t)]^{-1} \cdot \nabla_0\mathbf{r}(t) \\ &= [\nabla_0\mathbf{r}(t)]^\top \cdot \mathbf{C}_u^{-1}(t) \cdot \nabla_0\mathbf{r}(t). \end{aligned} \quad (19)$$

Our purpose now is to determine the derivatives of the principal invariants, I_k ($k = 1, 2$), of the tensor $\mathbf{C}_e(t)$ with respect to time. Differentiation of Eq. (16) results in

$$\begin{aligned} \frac{d\mathbf{C}_e}{dt}(t) &= \frac{d}{dt}[\nabla_0\mathbf{r}_u(t)]^{-1} \cdot \mathbf{C}(t) \cdot [\nabla_0\mathbf{r}_u(t)]^{-\top} \\ &\quad + [\nabla_0\mathbf{r}_u(t)]^{-1} \cdot \frac{d\mathbf{C}}{dt}(t) \cdot [\nabla_0\mathbf{r}_u(t)]^{-\top} \\ &\quad + [\nabla_0\mathbf{r}_u(t)]^{-1} \cdot \mathbf{C}(t) \cdot \frac{d}{dt}[\nabla_0\mathbf{r}_u(t)]^{-\top}. \end{aligned} \quad (20)$$

Bearing in mind that

$$\frac{d\mathbf{r}_u}{dt}(t) = \mathbf{v}_u(t),$$

where $\mathbf{v}_u(t)$ is the velocity vector for sliding of junctions, and using the chain rule for differentiation, we obtain

$$\frac{d}{dt}[\nabla_0\mathbf{r}_u(t)] = \nabla_0\mathbf{v}_u(t) = \nabla_0\mathbf{r}_u(t) \cdot \mathbf{L}_u(t), \quad (21)$$

where

$$\mathbf{L}_u(t) = \nabla_u(t)\mathbf{v}_u(t).$$

Taking into account that

$$\frac{d}{dt}[\nabla_0\mathbf{r}_u(t)]^{-1} = -[\nabla_0\mathbf{r}_u(t)]^{-1} \cdot \frac{d}{dt}[\nabla_0\mathbf{r}_u(t)] \cdot [\nabla_0\mathbf{r}_u(t)]^{-1},$$

we find from Eq. (21) that

$$\frac{d}{dt}[\nabla_0\mathbf{r}_u(t)]^{-1} = -\mathbf{L}_u(t) \cdot [\nabla_0\mathbf{r}_u(t)]^{-1}. \quad (22)$$

It follows from Eq. (13) that the derivative of the Cauchy deformation tensor $\mathbf{C}(t)$ reads

$$\frac{d\mathbf{C}}{dt}(t) = \nabla_0\mathbf{v}(t) \cdot [\nabla_0\mathbf{r}(t)]^\top + \nabla_0\mathbf{r}(t) \cdot [\nabla_0\mathbf{v}(t)]^\top, \quad (23)$$

where

$$\mathbf{v}(t) = \frac{d\mathbf{r}}{dt}(t)$$

is the velocity vector. Taking into account that

$$\nabla_0 \mathbf{v}(t) = \nabla_0 \mathbf{r}(t) \cdot \nabla(t) \mathbf{v}(t),$$

where $\nabla(t)$ is the gradient operator in the deformed configuration, we arrive at the formula

$$\frac{d\mathbf{C}}{dt}(t) = 2\nabla_0 \mathbf{r}(t) \cdot \mathbf{D}(t) \cdot [\nabla_0 \mathbf{r}(t)]^\top, \quad (24)$$

where

$$\mathbf{L}(t) = \nabla(t) \mathbf{v}(t)$$

is the velocity gradient and

$$\mathbf{D}(t) = \frac{1}{2} [\mathbf{L}(t) + \mathbf{L}^\top(t)],$$

is the rate-of-strain tensor. Equations (16), (20), (22) and (24) result in

$$\begin{aligned} \frac{d\mathbf{C}_e}{dt}(t) &= -\mathbf{L}_u(t) \cdot \mathbf{C}_e(t) - \mathbf{C}_e(t) \cdot \mathbf{L}_u^\top(t) \\ &\quad + 2[\nabla_0 \mathbf{r}_u(t)]^{-1} \cdot \nabla_0 \mathbf{r}(t) \cdot \mathbf{D}(t) \cdot [\nabla_0 \mathbf{r}(t)]^\top \cdot [\nabla_0 \mathbf{r}_u(t)]^{-\top}. \end{aligned} \quad (25)$$

Bearing in mind that

$$\frac{d\mathbf{C}_e^{-1}}{dt}(t) = -\mathbf{C}_e^{-1}(t) \cdot \frac{d\mathbf{C}_e}{dt}(t) \cdot \mathbf{C}_e^{-1}(t),$$

we find from Eqs. (16) and (25) that

$$\begin{aligned} \frac{d\mathbf{C}_e^{-1}}{dt}(t) &= \mathbf{C}_e^{-1}(t) \cdot \mathbf{L}_u(t) + \mathbf{L}_u^\top(t) \cdot \mathbf{C}_e^{-1}(t) \\ &\quad - 2[\nabla_0 \mathbf{r}_u(t)]^\top \cdot \mathbf{C}_e^{-1}(t) \cdot \nabla_0 \mathbf{r}(t) \cdot \mathbf{D}(t) \cdot [\nabla_0 \mathbf{r}(t)]^\top \cdot \mathbf{C}_e^{-1}(t) \cdot \nabla_0 \mathbf{r}_u(t). \end{aligned} \quad (26)$$

The first principal invariant of the tensor $\mathbf{C}_e(t)$ is given by

$$I_1(\mathbf{C}_e) = \mathbf{C}_e : \mathbf{I},$$

where the colon stands for convolution. Differentiating this equality with respect to time and using Eq. (25), we obtain

$$\begin{aligned} \frac{dI_1}{dt}(\mathbf{C}_e(t)) &= -\mathbf{L}_u(t) : \mathbf{C}_e(t) - \mathbf{C}_e(t) : \mathbf{L}_u^\top(t) \\ &\quad + 2[(\nabla_0 \mathbf{r}(t))^\top \cdot (\nabla_0 \mathbf{r}_u(t))^{-\top} \cdot (\nabla_0 \mathbf{r}_u(t))^{-1} \cdot \nabla_0 \mathbf{r}(t)] : \mathbf{D}(t). \end{aligned}$$

Combining this equality with Eq. (14) and introducing the rate-of-strain tensor for sliding of junctions

$$\mathbf{D}_u(t) = \frac{1}{2} [\mathbf{L}_u(t) + \mathbf{L}_u^\top(t)],$$

we arrive at the formula

$$\frac{dI_1}{dt}(\mathbf{C}_e(t)) = 2[(\nabla_0 \mathbf{r}(t))^\top \cdot \mathbf{C}_u^{-1}(t) \cdot \nabla_0 \mathbf{r}(t)] : \mathbf{D}(t) - 2\mathbf{C}_e(t) : \mathbf{D}_u(t). \quad (27)$$

It follows from Eqs. (19) and (27) that

$$\frac{dI_1}{dt}(\mathbf{C}_e(t)) = 2[\mathbf{B}_e(t) : \mathbf{D}(t) - \mathbf{C}_e(t) : \mathbf{D}_u(t)]. \quad (28)$$

The Cauchy deformation tensors for transitions from the reference state to the deformed state and from the reference state to the unloaded state are assumed to obey the incompressibility condition, which implies that

$$I_3(\mathbf{C}_e) = 1.$$

It follows from this equality that

$$I_2(\mathbf{C}_e(t)) = I_1(\mathbf{C}_e^{-1}(t)) = \mathbf{C}_e^{-1}(t) : \mathbf{I}. \quad (29)$$

We differentiate Eq. (29) with respect to time, use Eqs. (13), (14) and (26), and obtain

$$\begin{aligned} \frac{dI_2}{dt}(\mathbf{C}_e(t)) &= \mathbf{C}_e^{-1}(t) : \mathbf{L}_u(t) + \mathbf{L}_u^\top(t) : \mathbf{C}_e^{-1}(t) - 2\mathbf{D}(t) : \\ &\quad \left[(\nabla_0 \mathbf{r}(t))^\top \cdot \mathbf{C}^{-1}(t) \cdot \nabla_0 \mathbf{r}_u(t) \cdot (\nabla_0 \mathbf{r}_u(t))^\top \cdot \mathbf{C}^{-1}(t) \cdot \nabla_0 \mathbf{r}(t) \right] \\ &= 2\mathbf{C}_e^{-1}(t) : \mathbf{D}_u(t) - 2 \left[(\nabla_0 \mathbf{r}(t))^{-1} \cdot \mathbf{C}_u(t) \cdot (\nabla_0 \mathbf{r}(t))^{-\top} \right] : \mathbf{D}(t). \end{aligned}$$

This equality together with Eq. (19) results in the formula

$$\frac{dI_2}{dt}(\mathbf{C}_e(t)) = -2[\mathbf{B}_e^{-1} : \mathbf{D}(t) - \mathbf{C}_e^{-1}(t) : \mathbf{D}_u(t)]. \quad (30)$$

Equations (28) and (30) determine the derivatives of the principal invariants of the tensor $\mathbf{C}_e(t)$.

Our goal now is to calculate the derivative of an arbitrary smooth function, $\phi = \phi(I_1, I_2)$, of the principal invariants, I_k , of the Cauchy deformation tensor, $\mathbf{C}_e(t)$, with respect to time. According to the chain rule for differentiation,

$$\frac{d\phi}{dt} = \phi_{,1}(I_1, I_2) \frac{dI_1}{dt} + \phi_{,2}(I_1, I_2) \frac{dI_2}{dt} \quad (31)$$

with

$$\phi_{,k} = \frac{\partial \phi}{\partial I_k}.$$

Substitution of expressions (28) and (30) into Eq. (31) implies that

$$\begin{aligned} \frac{d\phi}{dt}(I_1(\mathbf{C}_e(t)), I_2(\mathbf{C}_e(t))) &= 2[\phi_{,1}\mathbf{B}_e(t) - \phi_{,2}\mathbf{B}_e^{-1}(t)] : \mathbf{D}(t) \\ &\quad - 2[\phi_{,1}\mathbf{C}_e(t) - \phi_{,2}\mathbf{C}_e^{-1}(t)] : \mathbf{D}_u(t). \end{aligned} \quad (32)$$

Equation (32) generalizes the conventional formula for the derivative of a function ϕ of the principal invariants, I_k , of the Cauchy deformation tensor $\mathbf{C}(t)$,

$$\frac{d\phi}{dt}(I_1(\mathbf{C}(t)), I_2(\mathbf{C}(t))) = 2[\phi_{,1}\mathbf{B}(t) - \phi_{,2}\mathbf{B}^{-1}(t)] : \mathbf{D}(t). \quad (33)$$

In what follows, we analyze deformation of meso-domains with various potential energies, ω , where junctions start to slip with respect to the bulk material at various times, τ , while they moved together with the bulk medium before the instant τ . This means that the tensors \mathbf{B}_e and \mathbf{C}_e become functions of three variables, t , τ and ω , that satisfy the initial conditions

$$\mathbf{B}_e(t, \tau, \omega)|_{t=\tau} = \mathbf{B}(\tau), \quad \mathbf{C}_e(t, \tau, \omega)|_{t=\tau} = \mathbf{C}(\tau). \quad (34)$$

It follows from Eq. (32) that the derivative of an arbitrary function ϕ of the first two principal invariants of the Cauchy deformation tensor $\mathbf{C}_e(t, \tau)$ reads

$$\begin{aligned} \frac{\partial \phi}{\partial t} & \left(I_1(\mathbf{C}_e(t, \tau, \omega)), I_2(\mathbf{C}_e(t, \tau, \omega)) \right) \\ &= 2 \left[\phi_{,1} \mathbf{B}_e(t, \tau, \omega) - \phi_{,2} \mathbf{B}_e^{-1}(t, \tau, \omega) \right] : \mathbf{D}(t) \\ & \quad - 2 \left[\phi_{,1} \mathbf{C}_e(t, \tau, \omega) - \phi_{,2} \mathbf{C}_e^{-1}(t, \tau, \omega) \right] : \mathbf{D}_u(t, \tau, \omega). \end{aligned} \quad (35)$$

Equations (33) and (35) will be used in the next section to calculate the derivative of the mechanical energy of a filled elastomer with respect to time.

4 Strain energy of an elastomer

We confine ourselves to loading processes that increase the concentration of active meso-domains with time. This implies that any active region can be entirely characterized by its potential energy, ω , and the instant, τ , when it became active. We set $\tau = 0$ for meso-domains active in the stress-free state.

The conventional affinity hypothesis is adopted for deformation of passive meso-domains. This assumption disregards thermal oscillations of junctions and postulates that the deformation gradient for the motion of junctions at the micro-level coincides with that for the movement of appropriate points of an elastomer at the macro-level (Treloar, 1975).

A passive region is treated as an isotropic incompressible medium whose mechanical energy per strand, w , depends on the current temperature, T (the strong effect of temperature reflects the entropic nature of the strain energy for rubbery polymers), the measure of damage, α , and the first two principal invariants, I_k , of the right Cauchy deformation tensor \mathbf{C} ,

$$w = w(\alpha(t), T(t), I_1(\mathbf{C}(t)), I_2(\mathbf{C}(t))). \quad (36)$$

At an arbitrary instant $t \geq 0$, the strain energy of a strand, w_0 , belonging to a meso-domain with potential energy ω which became active at instant $\tau \in [0, t]$ is assumed to be a function of the current temperature, T , and the first two principal invariants of the right Cauchy deformation tensor \mathbf{C}_e ,

$$w_0 = w_0(T(t), I_1(\mathbf{C}_e(t, \tau, \omega)), I_2(\mathbf{C}_e(t, \tau, \omega))). \quad (37)$$

Equations (36) and (37) are based on the conventional hypothesis that the excluded-volume effect and other multi-chain effects are screened for an individual chain by surrounding macromolecules and they may be accounted for in terms of the incompressibility condition (Everaers, 1998).

To simplify the analysis, the strain energy of a strand is assumed to be independent of the potential energy, ω , of a meso-region to which this strand belongs (the latter means that the functions w and w_0 are treated as average mechanical energies of strands). The mechanical energy of a strand in an active meso-region, w_0 , differs, however, from the strain energy, w , of a strand in a passive domain. The mechanical energy of a passive meso-domain with a potential energy ω and a damage measure α reads

$$w(\alpha, T, I_1, I_2) = w_0(T, I_1, I_2) + \alpha \Delta w(T, I_1, I_2), \quad (38)$$

where Δw is the increment of strain energy per strand in a passive meso-domain (with respect to that in an active region) caused by inter-chain interactions (van der Waals forces). Equation (38) implies that the strain energy density of an elastomer is continuous at the point of transition of a passive meso-domain into the active state (when the damage parameter, α , vanishes).

Summing the mechanical energies of strands belonging to initial active meso-regions with various potential energies, ω , to passive meso-domains with various energies, ω , and damage measures, α , as well as to meso-domains that become active at various instants, $\tau \in [0, t]$, we find the strain energy density per unit mass of an elastomer

$$\begin{aligned} W(t) = & \int_0^\infty d\omega \left[\int_0^\infty \Xi_p(t, \alpha, \omega) w(\alpha, T(t), I_1(\mathbf{C}(t)), I_2(\mathbf{C}(t))) d\alpha \right. \\ & + X_a(0, \omega) w_0(T(t), I_1(\mathbf{C}_e(t, 0, \omega)), I_2(\mathbf{C}_e(t, 0, \omega))) \\ & \left. + \int_0^t \gamma(\tau, \omega) w_0(T(t), I_1(\mathbf{C}_e(t, \tau, \omega)), I_2(\mathbf{C}_e(t, \tau, \omega))) d\tau \right]. \end{aligned}$$

Substitution of Eqs. (36) to (38) into this equality results in

$$\begin{aligned} W(t) = & N_p(t) w_0(T(t), I_1(\mathbf{C}(t)), I_2(\mathbf{C}(t))) + Z(t) \Delta w(T(t), I_1(\mathbf{C}(t)), I_2(\mathbf{C}(t))) \\ & + \int_0^\infty d\omega \left[X_a(0, \omega) w_0(T(t), I_1(\mathbf{C}_e(t, 0, \omega)), I_2(\mathbf{C}_e(t, 0, \omega))) \right. \\ & \left. + \int_0^t \gamma(\tau, \omega) w_0(T(t), I_1(\mathbf{C}_e(t, \tau, \omega)), I_2(\mathbf{C}_e(t, \tau, \omega))) d\tau \right], \end{aligned} \quad (39)$$

where the function $N_p(t)$ is given by Eqs. (6) and (7) and

$$Z(t) = \int_0^\infty \alpha d\alpha \int_0^\infty \Xi_p(t, \alpha, \omega) d\omega. \quad (40)$$

Our purpose now is to calculate the derivative of the function $W(t)$ with respect to time. It follows from Eqs. (7), (33) to (35) and (39) that

$$\frac{dW}{dt}(t) = J(t) \frac{dT}{dt}(t) + 2\mathbf{\Lambda}(t) : \mathbf{D}(t) - Y_1(t) - Y_2(t), \quad (41)$$

where

$$J(t) = N_p(t) \frac{\partial w_0}{\partial T}(T(t), I_1(\mathbf{C}(t)), I_2(\mathbf{C}(t))) + Z(t) \frac{\partial \Delta w}{\partial T}(T(t), I_1(\mathbf{C}(t)), I_2(\mathbf{C}(t)))$$

$$\begin{aligned}
& + \int_0^\infty d\omega \left[X_a(0, \omega) \frac{\partial w_0}{\partial T} (T(t), I_1(\mathbf{C}_e(t, 0, \omega)), I_2(\mathbf{C}_e(t, 0, \omega))) \right. \\
& \left. + \int_0^t \gamma(\tau, \omega) \frac{\partial w_0}{\partial T} (T(t), I_1(\mathbf{C}_e(t, \tau, \omega)), I_2(\mathbf{C}_e(t, \tau, \omega))) d\tau \right], \\
\mathbf{\Lambda}(t) &= N_p(t) \left(w_{0,1} (T(t), I_1(\mathbf{C}(t)), I_2(\mathbf{C}(t))) \mathbf{B}(t) \right. \\
& \quad \left. - w_{0,2} (T(t), I_1(\mathbf{C}(t)), I_2(\mathbf{C}(t))) \mathbf{B}^{-1}(t) \right) \\
& \quad + Z(t) \left(\Delta w_{,1} (T(t), I_1(\mathbf{C}(t)), I_2(\mathbf{C}(t))) \mathbf{B}(t) \right. \\
& \quad \left. - \Delta w_{,2} (T(t), I_1(\mathbf{C}(t)), I_2(\mathbf{C}(t))) \mathbf{B}^{-1}(t) \right) \\
& \quad + \int_0^\infty d\omega \left[X_a(0, \omega) \left(w_{0,1} (T(t), I_1(\mathbf{C}_e(t, 0, \omega)), I_2(\mathbf{C}_e(t, 0, \omega))) \mathbf{B}_e(t, 0, \omega) \right. \right. \\
& \quad \left. \left. - w_{0,2} (T(t), I_1(\mathbf{C}_e(t, 0, \omega)), I_2(\mathbf{C}_e(t, 0, \omega))) \mathbf{B}_e^{-1}(t, 0, \omega) \right) \right. \\
& \quad \left. + \int_0^t \gamma(\tau, \omega) \left(w_{0,1} (T(t), I_1(\mathbf{C}_e(t, \tau, \omega)), I_2(\mathbf{C}_e(t, \tau, \omega))) \mathbf{B}_e(t, \tau, \omega) \right. \right. \\
& \quad \left. \left. - w_{0,2} (T(t), I_1(\mathbf{C}_e(t, \tau, \omega)), I_2(\mathbf{C}_e(t, \tau, \omega))) \mathbf{B}_e^{-1}(t, \tau, \omega) \right) d\tau \right], \\
Y_1(t) &= -\frac{dN_p}{dt}(t) w_0 (T(t), I_1(\mathbf{C}(t)), I_2(\mathbf{C}(t))) \\
& \quad - \frac{dZ}{dt}(t) \Delta w (T(t), I_1(\mathbf{C}(t)), I_2(\mathbf{C}(t))) \\
& \quad - \int_0^\infty \gamma(t, \omega) w_0 (T(t), I_1(\mathbf{C}_e(t, t, \omega)), I_2(\mathbf{C}_e(t, t, \omega))) d\omega, \\
Y_2(t) &= 2 \int_0^\infty \left[X_a(0, \omega) \mathbf{\Lambda}_u(t, 0, \omega) : \mathbf{D}_u(t, 0, \omega) \right. \\
& \quad \left. + \int_0^t \gamma(\tau, \omega) \mathbf{\Lambda}_u(t, \tau, \omega) : \mathbf{D}_u(t, \tau, \omega) d\tau \right] d\omega. \tag{42}
\end{aligned}$$

The function $\mathbf{\Lambda}_u$ reads

$$\begin{aligned}
\mathbf{\Lambda}_u(t, \tau, \omega) &= w_{0,1} (T(t), I_1(\mathbf{C}_e(t, \tau, \omega)), I_2(\mathbf{C}_e(t, \tau, \omega))) \mathbf{C}_e(t, \tau, \omega) \\
& \quad - w_{0,2} (T(t), I_1(\mathbf{C}_e(t, \tau, \omega)), I_2(\mathbf{C}_e(t, \tau, \omega))) \mathbf{C}_e^{-1}(t, \tau, \omega). \tag{43}
\end{aligned}$$

Equations (7), (9), (34) and (42) imply that

$$Y_1(t) = -\frac{dZ}{dt}(t) \Delta w (T(t), I_1(\mathbf{C}(t)), I_2(\mathbf{C}(t))), \tag{44}$$

which means that the function Y_1 is non-negative for an arbitrary program of loading with an increasing number of active meso-domains.

5 Constitutive equations

We confine ourselves to quasi-static loadings with finite strains, when mechanically induced changes in temperature, ΔT , are rather weak. This implies that the effect of

temperature on the specific heat, c , may be disregarded. The following expression is adopted for the free energy (per unit mass) of a filled elastomer:

$$\Psi = \Psi_0 + (c - S_0)(T - T_0) - cT \ln \frac{T}{T_0} + W, \quad (45)$$

where Ψ_0 and S_0 are the free energy and the entropy per unit mass in the stress-free state at the reference temperature T_0 . The second and third terms on the right-hand side of Eq. (45) characterize the free energy of thermal motion of chains.

For an incompressible medium, the Clausius–Duhem inequality reads (Haupt, 2000)

$$Q = -S \frac{dT}{dt} - \frac{d\Psi}{dt} + \frac{1}{\rho} \left(\boldsymbol{\Sigma}' : \mathbf{D} - \frac{1}{T} \mathbf{q} \cdot \nabla T \right) \geq 0, \quad (46)$$

where ρ is mass density, $\boldsymbol{\Sigma}'$ is the deviatoric component of the Cauchy stress tensor $\boldsymbol{\Sigma}$, \mathbf{q} is the heat flux vector, S is the entropy, and Q is the internal dissipation per unit mass. Substitution of Eqs. (41) and (45) into Eq. (46) results in

$$\begin{aligned} Q = & - \left(S - S_0 - c \ln \frac{T}{T_0} + J \right) \frac{dT}{dt} + \frac{1}{\rho} \left(\boldsymbol{\Sigma}' - 2\rho\boldsymbol{\Lambda} \right) : \mathbf{D} \\ & + Y_1 + Y_2 - \frac{1}{\rho T} \mathbf{q} \cdot \nabla T \geq 0. \end{aligned} \quad (47)$$

The function Y_1 describes the energy dissipation driven by transition of passive mesodomains into the active state, Y_2 characterizes the entropy production induced by slippage of junctions with respect to the bulk material, whereas the last term in Eq. (47) is responsible for internal dissipation caused by thermal conductivity.

Because Eq. (47) is to be satisfied for an arbitrary loading, the expressions in brackets vanish. This implies the formula for the entropy per unit mass

$$S(t) = S_0 + c \ln \frac{T(t)}{T_0} - J(t)$$

and the constitutive equation

$$\boldsymbol{\Sigma}(t) = -P(t)\mathbf{I} + 2\rho\boldsymbol{\Lambda}(t),$$

where P is pressure. Substitution of expression (42) into this equality implies the stress–strain relation

$$\begin{aligned} \boldsymbol{\Sigma}(t) = & -P(t)\mathbf{I} + 2\rho \left\{ N_p(t) \left(w_{0,1}(T(t), I_1(\mathbf{C}(t)), I_2(\mathbf{C}(t))) \mathbf{B}(t) \right. \right. \\ & \left. \left. - w_{0,2}(T(t), I_1(\mathbf{C}(t)), I_2(\mathbf{C}(t))) \mathbf{B}^{-1}(t) \right) \right. \\ & + Z(t) \left(\Delta w_{,1}(T(t), I_1(\mathbf{C}(t)), I_2(\mathbf{C}(t))) \mathbf{B}(t) \right. \\ & \left. \left. - \Delta w_{,2}(T(t), I_1(\mathbf{C}(t)), I_2(\mathbf{C}(t))) \mathbf{B}^{-1}(t) \right) \right. \\ & \left. + \int_0^\infty \left[X_a(0, \omega) \left(w_{0,1}(T(t), I_1(\mathbf{C}_e(t, 0, \omega)), I_2(\mathbf{C}_e(t, 0, \omega))) \mathbf{B}_e(t, 0, \omega) \right. \right. \right. \end{aligned}$$

$$\begin{aligned}
& -w_{0,2} \left(T(t), I_1(\mathbf{C}_e(t, 0, \omega)), I_2(\mathbf{C}_e(t, 0, \omega)) \right) \mathbf{B}_e^{-1}(t, 0, \omega) \Big) \\
& + \int_0^t \gamma(\tau, \omega) \left(w_{0,1} \left(T(t), I_1(\mathbf{C}_e(t, \tau, \omega)), I_2(\mathbf{C}_e(t, \tau, \omega)) \right) \mathbf{B}_e(t, \tau, \omega) \right. \\
& \left. - w_{0,2} \left(T(t), I_1(\mathbf{C}_e(t, \tau, \omega)), I_2(\mathbf{C}_e(t, \tau, \omega)) \right) \mathbf{B}_e^{-1}(t, \tau, \omega) \right) d\tau \Big] d\omega \Big\}. \quad (48)
\end{aligned}$$

We adopt the Fourier law for the heat flux vector \mathbf{q} ,

$$\mathbf{q} = -\kappa \nabla T,$$

where $\kappa > 0$ is thermal diffusivity. It follows from this equation that the last term on the right-hand side of Eq. (47) is non-negative.

The incompressibility condition implies that the first invariant of the rate-of-strain tensor \mathbf{D}_u vanishes, which means that

$$\mathbf{\Lambda}_u : \mathbf{D}_u = \mathbf{\Lambda}'_u : \mathbf{D}_u,$$

where the prime stands for the deviatoric component of a tensor. By analogy with Eq. (1), we postulate that the rate-of-strain tensor for sliding of junctions, \mathbf{D}_u , is proportional to the tensor $\mathbf{\Lambda}'_u$,

$$\rho \mathbf{\Lambda}'_u(t, \tau, \omega) = \eta \mathbf{D}_u(t, \tau, \omega), \quad (49)$$

where $\eta > 0$ is a viscosity. Equation (49) provides the flow rule for slippage of junctions with respect to the bulk material, which ensures that the term $\mathbf{\Lambda}_u : \mathbf{D}_u$ is non-negative. It follows from this result and Eq. (42) that $Y_2 \geq 0$ for an arbitrary program of straining. Because the function Y_1 is non-negative as well, governing equations (48) and (49) guarantee that the dissipation inequality (47) is fulfilled.

It follows from Eqs. (2), (4), (42) and (49) that

$$\begin{aligned}
\mathbf{D}_u(t, \tau, \omega) &= \frac{\rho \Gamma_0}{G} \exp(-\omega) \left[w_{0,1} \left(T(t), I_1(\mathbf{C}_e(t, \tau, \omega)), I_2(\mathbf{C}_e(t, \tau, \omega)) \right) \mathbf{C}'_e(t, \tau, \omega) \right. \\
&\quad \left. - w_{0,2} \left(T(t), I_1(\mathbf{C}_e(t, \tau, \omega)), I_2(\mathbf{C}_e(t, \tau, \omega)) \right) \left(\mathbf{C}_e^{-1}(t, \tau, \omega) \right)' \right]. \quad (50)
\end{aligned}$$

Formulas (48) and (50) entirely determine the evolution of an ensemble of meso-regions in a filled elastomer. These equations may be noticeably simplified provided that the conventional theory of rubber elasticity is applied to the description of the mechanical energy in active meso-domains. Setting

$$\rho w_0 = G(I_1 - 3), \quad (51)$$

which corresponds to the strain energy density of a neo-Hookean material, we find that

$$\begin{aligned}
\Sigma(t) &= -P(t) \mathbf{I} + 2G \left\{ N_p(t) \mathbf{B}(t) + \int_0^\infty \left[X_a(0, \omega) \mathbf{B}_e(t, 0, \omega) \right. \right. \\
&\quad \left. \left. + \int_0^t \gamma(\tau, \omega) \mathbf{B}_e(t, \tau, \omega) d\tau \right] d\omega \right\} \\
&\quad + 2\rho Z(t) \left[\Delta w_{,1} \left(T(t), I_1(\mathbf{C}(t)), I_2(\mathbf{C}(t)) \right) \mathbf{B}(t) \right. \\
&\quad \left. - \Delta w_{,2} \left(T(t), I_1(\mathbf{C}(t)), I_2(\mathbf{C}(t)) \right) \mathbf{B}^{-1}(t) \right] \quad (52)
\end{aligned}$$

and

$$\mathbf{D}_u(t, \tau, \omega) = \Gamma_0 \exp(-\omega) \mathbf{C}'_e(t, \tau, \omega). \quad (53)$$

Constitutive equations (52) and (53) are applied in the next section to analyze stresses in a bar under tension.

6 Uniaxial tension of a specimen

Points of the bar refer to Cartesian coordinates $\{X_i\}$ in the stress-free state and to Cartesian coordinates $\{x_i\}$ in the deformed state, ($i = 1, 2, 3$). Uniaxial tension of an incompressible medium is described by the formulas

$$x_1 = k(t)X_1, \quad x_2 = k^{-\frac{1}{2}}(t)X_2, \quad x_3 = k^{-\frac{1}{2}}(t)X_3, \quad (54)$$

where $k = k(t)$ is the extension ratio. We assume that transition from the reference state to the unloaded state is determined by equations similar to Eq. (54),

$$\xi_1 = k_u(t, \tau, \omega)X_1, \quad \xi_2 = k_u^{-\frac{1}{2}}(t, \tau, \omega)X_2, \quad \xi_3 = k_u^{-\frac{1}{2}}(t, \tau, \omega)X_3, \quad (55)$$

where $\{\xi_i\}$ are Cartesian coordinates in the unloaded configuration and $k_u(t, \tau, \omega)$ is a function to be found. The Cauchy deformation tensors $\mathbf{B}(t)$ and $\mathbf{C}(t)$ read

$$\mathbf{B}(t) = \mathbf{C}(t) = k^2(t)\mathbf{e}_1\mathbf{e}_1 + k^{-1}(t)(\mathbf{e}_2\mathbf{e}_2 + \mathbf{e}_3\mathbf{e}_3), \quad (56)$$

where \mathbf{e}_i are base vectors of the frame $\{X_i\}$. The Cauchy deformation tensors $\mathbf{B}_e(t, \tau, \omega)$ and $\mathbf{C}_e(t, \tau, \omega)$ are given by

$$\mathbf{B}_e(t, \tau, \omega) = \mathbf{C}_e(t, \tau, \omega) = \left(\frac{k(t)}{k_u(t, \tau, \omega)}\right)^2 \mathbf{e}_1\mathbf{e}_1 + \frac{k_u(t, \tau, \omega)}{k(t)}(\mathbf{e}_2\mathbf{e}_2 + \mathbf{e}_3\mathbf{e}_3), \quad (57)$$

which implies that

$$\mathbf{C}'_e(t, \tau, \omega) = \frac{2}{3} \left[\left(\frac{k(t)}{k_u(t, \tau, \omega)}\right)^2 - \frac{k_u(t, \tau, \omega)}{k(t)} \right] \left[\mathbf{e}_1\mathbf{e}_1 - \frac{1}{2}(\mathbf{e}_2\mathbf{e}_2 + \mathbf{e}_3\mathbf{e}_3) \right]. \quad (58)$$

It follows from Eq. (55) that

$$\mathbf{D}_u(t, \tau, \omega) = \frac{1}{k_u(t, \tau, \omega)} \frac{\partial k_u}{\partial t}(t, \tau, \omega) \left[\mathbf{e}_1\mathbf{e}_1 - \frac{1}{2}(\mathbf{e}_2\mathbf{e}_2 + \mathbf{e}_3\mathbf{e}_3) \right]. \quad (59)$$

Substitution of expressions (58) and (59) into the flow rule (53) implies that the function $k_u(t, \tau, \omega)$ satisfies the differential equation

$$\frac{1}{k_u(t, \tau, \omega)} \frac{\partial k_u}{\partial t}(t, \tau, \omega) = \Gamma_* \exp(-\omega) \left[\left(\frac{k(t)}{k_u(t, \tau, \omega)}\right)^2 - \frac{k_u(t, \tau, \omega)}{k(t)} \right] \quad (60)$$

with the initial condition

$$k_u(t, \tau, \omega) \Big|_{t=\tau} = 1. \quad (61)$$

The coefficient Γ_* in Eq. (60) reads

$$\Gamma_* = \frac{2}{3}\Gamma_0.$$

It follows from Eqs. (52), (56) and (57) that the non-zero components, Σ_k , of the Cauchy stress tensor

$$\Sigma = \Sigma_1 \mathbf{e}_1 \mathbf{e}_1 + \Sigma_2 (\mathbf{e}_2 \mathbf{e}_2 + \mathbf{e}_3 \mathbf{e}_3)$$

are given by

$$\begin{aligned} \Sigma_1(t) &= -P(t) + 2\rho Z(t) [\Delta w_{,1} k^2(t) - \Delta w_{,2} k^{-2}(t)] + 2Gk^2(t) \left\{ N_p(t) \right. \\ &\quad \left. + \int_0^\infty [X_a(0, \omega) k_u^{-2}(t, 0, \omega) + \int_0^t \gamma(\tau, \omega) k_u^{-2}(t, \tau, \omega) d\tau] d\omega \right\}, \\ \Sigma_2(t) &= -P(t) + 2\rho Z(t) [\Delta w_{,1} k^{-1}(t) - \Delta w_{,2} k(t)] + 2Gk^{-1}(t) \left\{ N_p(t) \right. \\ &\quad \left. + \int_0^\infty [X_a(0, \omega) k_u(t, 0, \omega) + \int_0^t \gamma(\tau, \omega) k_u(t, \tau, \omega) d\tau] d\omega \right\}, \end{aligned}$$

where the arguments of the function Δw are omitted. Excluding the unknown pressure $P(t)$ from the expressions for Σ_k with the help of the boundary condition

$$\Sigma_2(t) = 0,$$

we find the longitudinal stress

$$\begin{aligned} \Sigma_1(t) &= 2 \left[GN_p(t) + \rho Z(t) (\Delta w_{,1} + k^{-1}(t) \Delta w_{,2}) \right] (k^2(t) - k^{-1}(t)) \\ &\quad + 2G \int_0^\infty \left[X_a(0, \omega) \left(\left(\frac{k(t)}{k_u(t, 0, \omega)} \right)^2 - \frac{k_u(t, 0, \omega)}{k(t)} \right) \right. \\ &\quad \left. + \int_0^t \gamma(\tau, \omega) \left(\left(\frac{k(t)}{k_u(t, \tau, \omega)} \right)^2 - \frac{k_u(t, \tau, \omega)}{k(t)} \right) d\tau \right] d\omega. \end{aligned} \quad (62)$$

Equations (60) to (62) determine the stress in a specimen for an arbitrary program of straining. To compare results of numerical simulation with experimental data, we focus on a tensile relaxation test with

$$k(t) = \begin{cases} 1, & t < 0, \\ \lambda, & t > 0, \end{cases} \quad (63)$$

where $\lambda > 1$ is a constant.

For the loading program (63), $\Delta w_{,1}$ and $\Delta w_{,2}$ become functions of λ only,

$$\Delta w_{,k} = \Delta w_{,k}(\lambda) \quad (k = 1, 2).$$

The concentration of active meso-regions is assumed to be altered at the instant $t = 0$ only, which implies that the function $\gamma(t, \omega)$ vanishes for any $t > 0$ and the quantities N_p and Z are entirely determined by the elongation ratio λ ,

$$N_p = N_p(\lambda), \quad Z = Z(\lambda).$$

The number, $X_a(0, \omega)$, of active meso-domains with a potential energy ω becomes a function of λ ,

$$X_a(0, \omega) = N_a(\lambda)p(\lambda, \omega),$$

where $N_a(\lambda)$ is the number of active regions at stretching to the elongation ratio λ , and $p(\lambda, \omega)$ is the distribution function for active meso-domains that satisfies the condition

$$\int_0^\infty p(\lambda, \omega) d\omega = 1. \quad (64)$$

For the relaxation test (63), the quantity $k_u(t, 0, \omega)$ also becomes a function of λ ,

$$k_u(t, 0, \omega) = h(t, \lambda, \omega).$$

Using Eqs. (10), (11) and introducing the notation,

$$\begin{aligned} \psi_1(\lambda) &= 2 \left[GN + \rho Z(\lambda) (\Delta w_{,1}(\lambda) + \lambda^{-1} \Delta w_{,2}(\lambda)) \right] (\lambda^2 - \lambda^{-1}), \\ \psi_2(\lambda) &= 2GN_a(\lambda) (\lambda^2 - \lambda^{-1}), \end{aligned} \quad (65)$$

we find from Eqs. (62) and (63) that

$$\Sigma_1(t, \lambda) = \psi_1(\lambda) - \psi_2(\lambda) \int_0^\infty [1 - f(t, \lambda, \omega)] p(\lambda, \omega) d\omega, \quad (66)$$

where

$$f(t, \lambda, \omega) = (\lambda^2 - \lambda^{-1})^{-1} \left[\left(\frac{\lambda}{h(t, \lambda, \omega)} \right)^2 - \frac{h(t, \lambda, \omega)}{\lambda} \right]. \quad (67)$$

It follows from Eqs. (60), (61) and (63) that the function $h(t, \lambda, \omega)$ obeys the differential equation

$$\frac{\partial h}{\partial t}(t, \lambda, \omega) = \Gamma_* \exp(-\omega) \left[\left(\frac{\lambda}{h(t, \lambda, \omega)} \right)^2 - \frac{h(t, \lambda, \omega)}{\lambda} \right] h(t, \lambda, \omega), \quad h(0, \lambda, \omega) = 1. \quad (68)$$

Equations (64) and (66) imply that the dimensionless ratio

$$R(t, \lambda) = \frac{\Sigma_1(t, \lambda)}{\Sigma_1(0, \lambda)}$$

is given by

$$R(t, \lambda) = 1 - A(\lambda) \int_0^\infty [1 - f(t, \lambda, \omega)] p(\lambda, \omega) d\omega, \quad (69)$$

where

$$A(\lambda) = \frac{\psi_2(\lambda)}{\psi_1(\lambda)}. \quad (70)$$

To fit experimental data, we employ the quasi-Gaussian distribution function

$$p(\lambda, \omega) = p_0(\lambda) \exp \left[-\frac{(\omega - \langle \omega(\lambda) \rangle_0)^2}{2\sigma^2(\lambda)} \right], \quad (71)$$

where $\langle\omega\rangle_0$ and σ are adjustable parameters and p_0 is determined by condition (64). Substitution of expression (71) into Eq. (69) results in

$$R(t, \lambda) = 1 - A(\lambda)p_0(\lambda) \int_0^\infty [1 - f(t, \lambda, \omega)] \left[-\frac{(\omega - \langle\omega(\lambda)\rangle_0)^2}{2\sigma^2(\lambda)} \right] d\omega.$$

Introducing the new variable, $z = \omega - \omega_*$, where $\omega_* = \ln \Gamma_*$, we obtain

$$R(t, \lambda) = 1 - A(\lambda)p_0(\lambda) \int_{-\omega_*}^\infty [1 - f(t, \lambda, z)] \left[-\frac{(z - \langle\omega(\lambda)\rangle)^2}{2\sigma^2(\lambda)} \right] dz,$$

where $\langle\omega\rangle = \langle\omega\rangle_0 - \omega_*$. Assuming the relative width of the quasi-Gaussian distribution,

$$\zeta = \frac{\sigma}{\langle\omega\rangle} \quad (72)$$

to be small compared to $\langle\omega\rangle$ (this hypothesis will be discussed later), we neglect the integral over the interval $[-\omega_*, 0]$ and find that

$$R(t, \lambda) = 1 - A(\lambda)p_0(\lambda) \int_0^\infty [1 - f(t, \lambda, z)] \left[-\frac{(z - \langle\omega(\lambda)\rangle)^2}{2\sigma^2(\lambda)} \right] dz, \quad (73)$$

where the function $f(t, \lambda, z)$ is determined by Eq. (67). According to Eq. (68), the function $h(t, \lambda, z)$ satisfies the differential equation

$$\frac{\partial h}{\partial t}(t, \lambda, z) = \exp(-z) \left[\left(\frac{\lambda}{h(t, \lambda, z)} \right)^2 - \frac{h(t, \lambda, z)}{\lambda} \right] h(t, \lambda, z), \quad h(0, \lambda, z) = 1. \quad (74)$$

Equations (73) and (74) are determined by 3 dimensionless parameters:

1. the ratio, A , of the relaxing stress to the total stress at the beginning of the relaxation test;
2. the average potential energy, $\langle\omega\rangle$, for sliding of junctions in active in meso-domains;
3. the standard deviation of the potential energy, σ .

7 Experimental procedure

Three series of uniaxial relaxation tests were performed at room temperature. Dumb-bell specimens were provided by TARRC laboratories (Hertford, UK) and were used as received. The tests were executed on specimens of the compound EDS-16 on the base of natural rubber reinforced by high abrasion furnace black. The compound contains 45 phr of carbon black with the mean diameter of filler particles of about 30 nm (Jäger and McQueen, 2001). A detailed formulation of the compound is presented in Table 1.

Experiments were carried out by using a testing machine designed at the Institute of Physics (Vienna, Austria) and equipped with a video-controlled system. To measure the longitudinal strain, two reflection lines were drawn in the central part of each specimen

before loading (with the distance 7 mm between them). Changes in the distance between these lines were measured by a video-extensometer (with the accuracy of about 1 %). The tensile force was measured by using a standard loading cell. The nominal stress was determined as the ratio of the axial force to the cross-sectional area of a specimen in the stress-free state, 4 mm \times 1 mm.

To analyze the effects of pre-loading and thermal recovery, the following testing procedure was chosen:

1. Any specimen was loaded with the strain rate $\dot{\epsilon}_+ = 3.0 \cdot 10^{-2} \text{ s}^{-1}$ up to a given elongation ratio λ , which was preserved constant during the relaxation test ($t_r = 1$ hour), and unloaded with the strain rate $\dot{\epsilon}_- = -\dot{\epsilon}_+$.
2. The specimen was annealed for $t_a = 24$ hours at room temperature.
3. The specimen was loaded with the strain rate $\dot{\epsilon}_+$ up to the elongation ratio $\lambda_{\max} = 4.0$ and unloaded with the strain rate $\dot{\epsilon}_-$.
4. The specimen was annealed for t_a at ambient temperature.
5. The specimen was loaded with the strain rate $\dot{\epsilon}_+$ up to the same elongation ratio, λ , as in the first test. This elongation ratio was preserved constant during the relaxation test, and, afterwards, the specimen was unloaded with the strain rate $\dot{\epsilon}_-$.
6. The specimen was recovered in an oven for 24 hours at the constant temperature $T = 100 \text{ }^\circ\text{C}$ and cooled down by air to room temperature for 4 hours.
7. The specimen was loaded with the strain rate $\dot{\epsilon}_+$ up to the same elongation ratio as in the first test. This elongation ratio was preserved constant during the relaxation test, and, afterwards, the specimen was unloaded with the strain rate $\dot{\epsilon}_-$.

The relaxation tests were carried out at four elongation ratios: $\lambda_1 = 2.0$, $\lambda_2 = 2.5$, $\lambda_3 = 3.0$, and $\lambda_4 = 3.5$.

The longitudinal stress σ was measured as a function of time t (the initial instant $t = 0$ corresponds to the beginning of the relaxation test). For any elongation ratio, λ , the dimensionless ratio $R(t, \lambda)$ is depicted versus the logarithm of time ($\log = \log_{10}$) in Figures 1 to 3.

These figures evidence that the longitudinal stress is noticeable decreased during the relaxation time, $t_r = 1$ h. For virgin specimens, this decrease equals 19.7 % at the elongation ratio λ_1 and it reaches 27.9 % at λ_4 .

After pre-loading to λ_{\max} and subsequent unloading, the time-dependent decrease in stress is weakened. The portion of the longitudinal stress relaxed during t_r is estimated as 14.4 % at the elongation ratio λ_1 and as 20.0 % at λ_4 .

Thermal recovery of specimens at the elevated temperature T for $t_a = 24$ h returns the specimens to their initial state. The decrease in the longitudinal stress during $t_r = 1$ h is estimated as 19.7 % at the smallest elongation ratio, λ_1 , and it grows up to 27.0 % at straining with λ_4 .

These changes in the time-dependent response of the CB filled natural rubber are associated with alternation of the internal structure of the compound at the micro-level:

1. the concentration of active domains per unit mass grows with an increase in the elongation ratio,
2. it is noticeably reduced under pre-loading and subsequent unloading,
3. the concentration of active meso-regions (practically) returns to its initial value after thermal recovery.

To verify these assertions, we determine adjustable parameters in Eqs. (73) and (74) by matching experimental data and analyze the effect of the longitudinal ratio, λ , on the coefficients A , $\langle\omega\rangle$ and σ .

8 Comparison with experimental data

Given an elongation ratio, λ , the fitting procedure consists in the following. We fix intervals $[0, \langle\omega\rangle_{\max}]$ and $[0, \sigma_{\max}]$ where the “best-fit” parameters $\langle\omega\rangle$ and σ are assumed to be found and divide these intervals into J subintervals by points $\langle\omega\rangle_j = j\Delta_\omega$ and $\sigma_j = j\Delta_\sigma$ with $j = 1, \dots, J$, $\Delta_\omega = \langle\omega\rangle_{\max}/J$ and $\Delta_\sigma = \sigma_{\max}/J$. For any pair of parameters $\langle\omega\rangle_i$ and σ_j , we find the constant p_0 from condition (64), where the integral is evaluated numerically. Afterwards, we calculate the integral in Eq. (73) and determine the pre-factor $A = A(i, j)$ [which ensures the best fit of the experimental curve $R_{\text{exp}}(t, \lambda)$] by the least-squares method. As a measure of deviations between observations and results of numerical analysis, we chose the function

$$r(i, j) = \sum_{t_k} \left[R_{\text{exp}}(t_k, \lambda) - R_{\text{num}}(t_k, \lambda) \right]^2, \quad (75)$$

where the sum is calculated over all experimental points depicted in Figures 1 to 3 and the function $R_{\text{num}}(t, \lambda)$ is determined by Eq. (73). Finally, the “best-fit” parameters $\langle\omega\rangle$ and σ are determined as those that minimize functional (75) on the set

$$\left\{ \langle\omega\rangle_i, \sigma_j \quad (i, j = 1, \dots, J) \right\}.$$

To ensure high accuracy in the approximation of observations, after determining the “optimal” parameters $\langle\omega\rangle_i$ and σ_j , the above procedure is repeated for the new intervals $[\langle\omega\rangle_{i-1}, \langle\omega\rangle_{i+1}]$ and $[\sigma_{j-1}, \sigma_{j+1}]$. In the numerical analysis, we set $\langle\omega\rangle_{\max} = 10.0$, $\sigma_{\max} = 10.0$ and $J = 20$. The integrals in Eqs. (64) and (73) are calculated by using Simpson’s method with 100 points and the step $\Delta z = 0.2$. For any z , the ordinary differential equation (74) is solved by the Runge-Kutta method with the time step $\Delta t = 0.05$ s.

To assess the effect of straining of the average potential energy for sliding, $\langle\omega\rangle$, and the standard deviation of energies, σ , we plot these quantities versus the first invariant, I_1 , of the Cauchy deformation tensor \mathbf{C} . It follows from Eq. (56) that in tensile relaxation tests,

$$I_1 = \lambda^2 + 2\lambda^{-1}.$$

Experimental data are approximated by the linear functions

$$\langle\omega\rangle = \omega_0 + \omega_1(I_1 - 3), \quad \sigma = \sigma_0 + \sigma_1(I_1 - 3), \quad (76)$$

where the coefficients ω_k and σ_k are determined by the least-squares technique. These parameters are listed in Table 2. Figures 4 and 5 show that phenomenological relations (76) ensure good accuracy of fitting.

To provide some physical basis for Eq. (76), we refer to Eq. (51) that implies that for a neo-Hookean medium, the difference $I_1 - 3$ may be treated a measure of the mechanical energy of active meso-regions. Equations (76) show that the parameters $\langle\omega\rangle$ and σ of the distribution function (71) for potential energies of active meso-domains are proportional to their average strain energy.

Equations (67) and (68) imply that $f(0, \lambda, \omega) = 1$ and $f(\infty, \lambda, \omega) = 0$. These equalities, together with Eqs. (64) and (66), yield

$$\Sigma_1(0, \lambda) = \psi_1(\lambda), \quad \Sigma_1(\infty, \lambda) = \psi_1(\lambda) - \psi_2(\lambda). \quad (77)$$

We associate $\Sigma_1(\infty, \lambda)$ with the equilibrium stress, $\Sigma_{\text{eq}}(\lambda)$, and $\Delta\Sigma(\lambda) = \Sigma_1(0, \lambda) - \Sigma_1(\infty, \lambda)$ with the relaxing stress. It follows from Eqs. (70) and (77) that the ratio

$$a(\lambda) = \frac{\Delta\Sigma(\lambda)}{\Sigma_{\text{eq}}(\lambda)} \quad (78)$$

reads

$$a(\lambda) = \frac{A(\lambda)}{1 - A(\lambda)}.$$

Given an elongation ratio λ , we find the dimensionless ratio $a(\lambda)$ from this equality, where the value of $A(\lambda)$ is determined by fitting observations, and plot a versus the first invariant, I_1 , of the Cauchy deformation tensor. Figure 6 demonstrates that the experimental data are correctly approximated by the linear relation

$$a = a_0 + a_1(I_1 - 3), \quad (79)$$

where the coefficients a_k (found by the least-squares algorithm) are collected in Table 2.

Figure 4 demonstrates that the average potential energy for sliding of junctions increases with the elongation ratio λ . This may be explained by the fact that only meso-domains with low potential energies are active in the stress-free state, whereas regions with higher potential energies become involved in the sliding process provided that sufficiently large tension is applied to the specimen. The rate of growth of the average potential energy for sliding, $\langle\omega\rangle$, with I_1 is relatively small for virgin specimens and it noticeably grows after pre-loading. After thermal recovery, changes in the function $\langle\omega\rangle(I_1)$ become similar to those for a virgin sample. The loading-unloading procedure with $\lambda_{\text{max}} = 4.0$ results in a decrease of the average potential energy of the ensemble of active meso-regions for a stress-free specimen (the parameter ω_0 is reduced by 8 %). This observation may be explained by (at least) two reasons:

1. damage of the rubbery compound during pre-loading “turns off” some active regions in a virgin sample that become passive under unloading;
2. stretching of a specimen to a high elongation ratio and subsequent unloading increase the rate of slippage of junctions with respect to the bulk medium. According to Eq. (68), this mechanically induced acceleration of the sliding process is tantamount to a decrease in the potential energy of active meso-regions.

Figure 5 shows that the standard deviation of potential energies, σ , increases with the elongation ratio, λ . This growth is rather modest for virgin and recovered samples, but it becomes stronger after pre-loading: the coefficient σ_1 for the pre-loaded specimens exceeds that for the virgin specimens by a factor of 6. After stretching of specimens to λ_{\max} and subsequent unloading, the quasi-Gaussian distribution of potential energies becomes substantially sharper: the standard deviation of energies for a stress-free rubbery compound, σ_0 , is decreased by 40 % compared to the virgin material. This may be explained by the fact that unloading induces transformation of active meso-domains with relatively high potential energies (which characterize a “tail” of the Gaussian function with large values of ω) into the passive state. Thermal recovery at an elevated temperature “activates” a part of these regions (the corresponding curve in Figure 5 is located higher than the curve for samples suffered pre-loading), but no total recovery is observed: the graph of the function $\sigma(I_1)$ for the recovered compound does not reach that for the virgin medium.

To evaluate the dimensionless width of the quasi-Gaussian distribution function (71), we calculate the ratio ζ with the help of Eq. (72) and plot it versus the first invariant, I_1 , of the Cauchy deformation tensor \mathbf{C} in Figure 7. Experimental data are approximated by the linear dependence

$$\zeta = \zeta_0 + \zeta_1(I_1 - 3), \quad (80)$$

where the constants ζ_0 and ζ_1 are determined by the least-squares algorithm. Figure 7 demonstrates fair agreement between the observations and the predictions of the phenomenological equation (80) with the parameters ζ_0 and ζ_1 listed in Table 2.

According to Figure 7, the dimensionless ratio ζ is located within the interval between 0.30 and 0.45 for all specimens, which implies that the width of the distribution function (71) is relatively small. The latter may be thought of as a confirmation of the assumptions employed in the derivation of Eq. (73). The quantity ζ slightly decreases with the elongation ratio λ for virgin and recovered specimens, and it weakly increases with λ for pre-loaded samples. The maximal width of the quasi-Gaussian distribution is observed for the virgin material. The distribution of potential energies for sliding of junctions in active meso-regions, $p(\omega)$, becomes sharper after pre-loading, whereas thermal recovery results in widening of this distribution.

The ratio of the relaxing stress to the equilibrium stress, a , is plotted in Figure 6 as a function of the extension ratio, λ . The parameter a is strongly influenced by stretching: for example, it grows by 45 % for virgin specimens when λ increases from 2.0 to 3.5. Equations (65), (77) and (78) imply that

$$a(\lambda) = \frac{N_a(\lambda)}{N_p(\lambda) + \rho G^{-1} Z(\lambda) [\Delta w_{,1}(\lambda) + \lambda^{-1} \Delta w_{,2}(\lambda)]}. \quad (81)$$

Because the term in brackets in Eq. (81) [the extra stress caused by inter-molecular interactions in passive meso-domains] is an increasing function of λ , the growth of $a(\lambda)$ is associated with the following phenomena occurring simultaneously:

1. micro-damage of passive meso-regions which results in a decrease of $Z(\lambda)$,

2. transformation of passive domains into the active state. The latter is equivalent to an increase in $N_a(\lambda)$ and a corresponding decrease in $N_p(\lambda)$ that is connected with $N_a(\lambda)$ by the conservation law (10).

To assess the effect of these two sources for changes in $a(\lambda)$, constitutive relations are necessary for damage of inter-chain links in passive meso-regions. A model for rupture of van der Waals links under loading will be the subject of a subsequent publication.

Stretching of samples to λ_{\max} and subsequent unloading result in a pronounced decrease in a that is partially recovered after annealing at an elevated temperature. The severe decrease in a (the ratio for the relaxing stress to the equilibrium stress in pre-loaded specimens at relatively small strains, a_0 , equals about 50 % of its value for virgin samples) reflects the decay of the relaxation process evidenced by comparison of curves plotted in Figures 1 and 2. This decrease in a is assumed to be closely connected with the Mullins effect observed in loading–unloading tests on particle-reinforced elastomers (see, e.g., Bouche, 1960, 1961; Govindjee and Simo, 1992; Bergström and Boyce, 1998; Miehe and Keck, 2000; Wu and Liechti, 2000, to mention a few).

It is worth noting a particular case of the model where the function Ξ_p is independent of time (or the current strain for a time-dependent program of loading). This implies that the parameters N_a , N_p and Z remain constants, and γ vanishes. Under these assumptions, the stress–strain relations (52) and (53) are reduced to the constitutive equations for a rheological model consisting of a nonlinear spring (which is characterized by the strain energy Δw of inter-chain interactions) connected in parallel with an infinite array of the Maxwell elements [neo–Hookean springs linked in series with nonlinear dashpots whose response is described by Eq. (53)]. A variant of the latter model with a finite number of Maxwell’s elements was widely used in the analysis of the viscoelastic and viscoplastic behavior of filler rubbers, see, e.g., Govindjee and Simo (1992), Kaliske and Rothert (1998), Miehe and Keck (2000), Haupt and Sedlan (2001). Fitting observations in the relaxation tests reveals that this simplified model does not capture noticeable changes in the parameters $\langle\omega\rangle$, σ and a under stretching. Our approach may be treated as an extension of the conventional rheological model, where the number of Maxwell’s elements and their viscosities are affected by mechanical factors.

9 Concluding remarks

Constitutive equations have been derived for the time-dependent behavior of particle-reinforced elastomers at finite strains. A filled rubber is modelled as an ensemble of meso-domains where junctions between chains (chemical and physical cross-links and entanglements) are not fixed in the bulk medium, but they can slip with respect to it. A mean-field approximation is employed to develop stress–strain relations: a complicated micro-structure of an elastomer reinforced with aggregates of filler is replaced by equivalent networks of macromolecules in meso-regions with various potential energies for sliding of junctions. The distribution of potential energies of these meso-domains reflects

1. impurities and local non-homogeneities in the spatial distribution of a cross-linker (which is typical of both unfilled and filled elastomers),

2. density fluctuations driven by segregation of short chains to the interfaces between filler particles and the host medium,
3. severe micro-stresses in the neighborhoods of filler clusters in a strained elastomer caused by the strong difference in the elastic moduli of filler and rubber.

It is assumed that junctions slip with respect to the bulk material in active meso-domains, and the rate of sliding is determined by Boltzmann's formula. Sliding of junctions in passive meso-regions is prevented by surrounding macromolecules (by means of inter-chain links that are partially ruptured under loading). The concentration of links that forbid sliding is described by a measure of micro-damage, α . Activation of a passive meso-domain occurs when the van der Waals forces between strands vanish that prevent sliding of junctions.

The mechanical energy of a filled elastomer is determined as the sum of strain energies of chains in active and passive meso-domains and the energy of interaction between macromolecules in passive regions. Constitutive equations for a filled elastomer are derived by using the laws of thermodynamics (the study is confined to the loading processes in which the concentration of active meso-regions does not decrease with time). These equations are applied for the analysis of stresses in an incompressible bar under uniaxial tension.

To validate the model, three series of tensile relaxation tests were performed on carbon black filled natural rubber at elongations up to 350 %. In the first series, virgin specimens are used, in the second series, relaxation experiments were carried out on the samples after mechanical pre-loading, and in the third series, the time-dependent response was measured on the same specimens after recovery at an elevated temperature. Figures 1 to 3 demonstrate fair agreement between the experimental data and the results of numerical simulation.

To describe quantitatively changes in the internal structure of a particle-reinforced elastomer induced by pre-loading and thermal recovery, the distribution of potential energies for sliding of junctions is approximated by a quasi-Gaussian function with two adjustable parameters. It is revealed that the average potential energy and the standard deviation of energies grow with the elongation ratio λ . After the loading-unloading procedure, these parameters are noticeably reduced. The latter is associated with rearrangement of active meso-domains driven by rupture of filler clusters. Thermal recovery implies that the parameters of the quasi-Gaussian distribution attempt to return to their values for virgin specimens, but they do not reach their initial values after annealing for $t_a = 24$ h at $T = 100$ °C.

Acknowledgement

We would like to express our gratitude to Dr. K. Fuller (TARRC, UK) for providing us with rubber specimens. Stimulating discussions with Profs. N. Aksel, A. Boukamel and S. Reese are gratefully acknowledged.

References

- Aksel, N., Hübner, Ch., 1996. The influence of dewetting in filled elastomers on the changes of their mechanical properties. *Arch. Appl. Mech.* 66, 231–241.
- Bergström, J.S., Boyce, M.C., 1998. Constitutive modelling of the large strain time-dependent behavior of elastomers. *J. Mech. Phys. Solids* 46, 931–954.
- Bueche, F., 1960. Molecular basis for the Mullins’ effect. *J. Appl. Polym. Sci.* 4, 107–114.
- Bueche, F., 1961. Mullins’ effect and rubber–filler interaction. *J. Appl. Polym. Sci.* 5, 271–281.
- Carlier, V., Sclavons, M., Jonas, A.M., Jerome, R., Legras, R., 2001. Probing thermoplastic matrix–carbon fiber interphases. 1. Preferential segregation of low molar mass chains to the interfaces. *Macromolecules* 34, 3725–3729.
- Clarke, S.M., Elias, F., Terentjev, E.M., 2000. Ageing of natural rubber under stress. *Eur. Phys. J. E* 2, 335–341.
- Dannenberg, E.M., 1975. The effects of surface chemical interactions on the properties of filler-reinforced rubbers. *Rubber Chem. Technol.* 48, 410–444.
- Desmorat, R., Cartournet, S., 2001. Thermodynamics modelling of internal friction and hysteresis of elastomers. In: Besdo, D., Schuster, R.H., Ihlemann, J. (Eds.), *Constitutive Models for Rubber II*. Swets and Zeitlinger, Lisse, pp. 37–43.
- Doi, M., Edwards, S.F., 1986. *The Theory of Polymer Dynamics*. Clarendon Press, Oxford.
- Drozdov, A.D., 1996. *Finite Elasticity and Viscoelasticity*. World Scientific, Singapore.
- Drozdov, A.D., 2001. A tube concept in finite viscoelasticity of rubbers. In: Besdo, D.; Schuster, R.H.; Ihlemann, J. (Eds.), *Constitutive Models for Rubber II*. Swets and Zeitlinger, Lisse, pp. 93–104.
- Drozdov, A.D., Dorfmann, A., 2001. Finite viscoelasticity of filled rubbers: the effects of pre-loading and thermal recovery. *cond-mat/0110269*.
- Everaers, R., 1998. Constrained fluctuation theories of rubber elasticity: general results and an exactly solvable model. *Eur. Phys. J. B* 4, 341–350.
- Govindjee, S., Simo, J.C., 1992. Mullins’ effect and the strain amplitude dependence of the storage modulus. *Int. J. Solids Structures* 29, 1737–1751.
- Green, M.S., Tobolsky, A.V., 1946. A new approach to the theory of relaxing polymeric media. *J. Chem. Phys.* 14, 80–92.
- Ha, K., Schapery, R.A., 1998. A three-dimensional viscoelastic constitutive model for particulate composites with growing damage and its experimental validation. *Int. J. Solids Structures* 35, 3497–3517.
- Hansen, D.E., 2000. A mesoscale strength model for silica-filled polydimethylsiloxane based on atomic forces obtained from molecular dynamics simulations. *J. Chem. Phys.* 113, 7656–7662.
- Haupt, P., 2000. *Continuum Mechanics and Theory of Materials*. Springer-Verlag, Berlin.
- Haupt, P., Sedlan, K., 2001. Viscoplasticity of elastomeric materials: experimental facts and constitutive modelling. *Arch. Appl. Mech.* 71, 89–109.

- Häusler, K., Sayir, M.B., 1995. Nonlinear viscoelastic response of carbon black reinforced rubber derived from moderately large deformations in torsion. *J. Mech. Phys. Solids* 43, 295–318.
- Herman, M.F., 2001. A length scale dependent model for stress relaxation in polymer melts. *Macromolecules* 34, 4580–4590.
- Holzappel, G., Simo, J., 1996. A new viscoelastic constitutive model for continuous media at finite thermomechanical changes. *Int. J. Solids Structures* 33, 3019–3034.
- Jäger, K.-M., McQueen, D.H., 2001. Fractal agglomerates and electric conductivity in carbon black polymer composites. *Polymer* 42, 9575–9581.
- Johnson, A.R., Stacer, R.G., 1993. Rubber viscoelasticity using the physically constrained system’s stretches as internal variables. *Rubber Chem. Technol.* 66, 567–577.
- Johnson, A.R., Quigley, J., Freese, C.E., 1995. A viscohyperelastic finite element model for rubber. *Comput. Methods Appl. Mech. Engng.* 127, 163–180.
- Kaliske, M., Rothert, H., 1998. Constitutive approach to rate-independent properties of filled elastomers. *Int. J. Solids Structures* 35, 2057–2071.
- Karasek, L., Sumita, M., 1996. Characterization of dispersion state of filler and polymer–filler interactions in rubber–carbon black composites. *J. Mater. Sci.* 31, 281–289.
- Leblanc, J.L., Cartault, M., 2001. Advanced torsional dynamic methods to study the morphology of uncured filled rubber compounds. *J. Appl. Polym. Sci.* 80, 2093–2104.
- Liang, J.Z., Li, R.K.Y., Tjong, S.C., 1999. Effects of glass bead content and surface treatment on viscoelasticity of filled polypropylene/elastomer hybrid composites. *Polym. Int.* 48, 1068–1072.
- Lion, A., 1996. A constitutive model for carbon black filled rubber: experimental investigations and mathematical representation. *Continuum Mech. Thermodyn.* 8, 153–169.
- Lion, A., 1997. On the large deformation behavior of reinforced rubber at different temperatures. *J. Mech. Phys. Solids* 45, 1805–1834.
- Lion, A., 1998. Thixotropic behaviour of rubber under dynamic loading histories: experiments and theory. *J. Mech. Phys. Solids* 46, 895–930.
- Lulei, F., Miehe, C., 2001. A physically-based constitutive model for finite viscoelastic deformations in rubbery polymers based on a directly evaluated micro–macro–transition. In: Besdo, D., Schuster, R.H., Ihlemann, J. (Eds.), *Constitutive Models for Rubber II*. Swets and Zeitlinger, Lisse, pp. 117–125.
- Miehe, C., 1995. Entropic thermo-elasticity at finite strains: aspects of the formulation and numerical implementation. *Comp. Meth. Appl. Mech. Engng.* 120, 243–269.
- Miehe, C., Keck, J., 2000. Superimposed finite elastic-viscoelastic-plastoelastic stress response with damage in filled rubbery polymers. Experiments, modelling and algorithmic implementation. *J. Mech. Phys. Solids* 48, 323–365.
- Phan-Thien, N., Tanner, R.L., 1977. A new constitutive equation derived from network theory. *J. Non-Newtonian Fluid Mech.* 2, 353–365.
- Phan-Thien, N., 1978. A nonlinear network viscoelastic model. *J. Rheol.* 22, 259–283.
- Reese, S., Govindjee, S., 1998. Theoretical and numerical aspects in the thermo-viscoelastic material behaviour of rubber-like polymers. *Mech. Time-Dependent Mater.* 1, 357–396.

Septanika, E.G., Ernst, L.J., 1998. Application of the network alteration theory for modeling the time-dependent constitutive behaviour of rubbers. 1. General theory. *Mech. Mater.* 30, 253–263. 2. Further evaluation of the general theory and experimental verification. *Mech. Mater.* 30, 265–273.

Spathis, G., 1997. Non-linear constitutive equations for viscoelastic behaviour of elastomers at large deformations. *Polym. Gels Networks* 5, 55–68.

Treloar, L.R.G., 1975. *The Physics of Rubber Elasticity*. Clarendon Press, Oxford.

Wu, J.-D., Liechti, K.M., 2000. Multiaxial and time dependent behavior of a filled rubber. *Mech. Time-Dependent Mater.* 4, 293–331.

Yatsuyanagi, F., Suzuki, N., Ito, M., Kaidou, H., 2001. Effects of secondary structure of fillers on the mechanical properties of silica filled rubber systems. *Polymer* 42, 9523–9529.

Table 1: Chemical composition of compound EDS-16 (phr by weight)

Formulation	Content
Natural rubber	100
Zinc oxide	5
Stearic acid	2
Carbon black (N330)	45
Process oil	4.5
Antidegradant(HPPD)	3
Antiozonant wax	2
Accelerator (CBS)	0.6
Sulphur	2.5

Table 2: Adjustable parameters of the model

Specimens	ω_0	ω_1	σ_0	σ_1	a_0	a_1	ζ_0	ζ_1
Virgin	7.508	0.109	3.252	0.017	0.296	0.028	0.423	-0.002
Preloaded	6.922	0.182	2.031	0.103	0.147	0.018	0.293	0.006
Recovered	7.397	0.134	2.871	0.019	0.280	0.025	0.375	-0.002

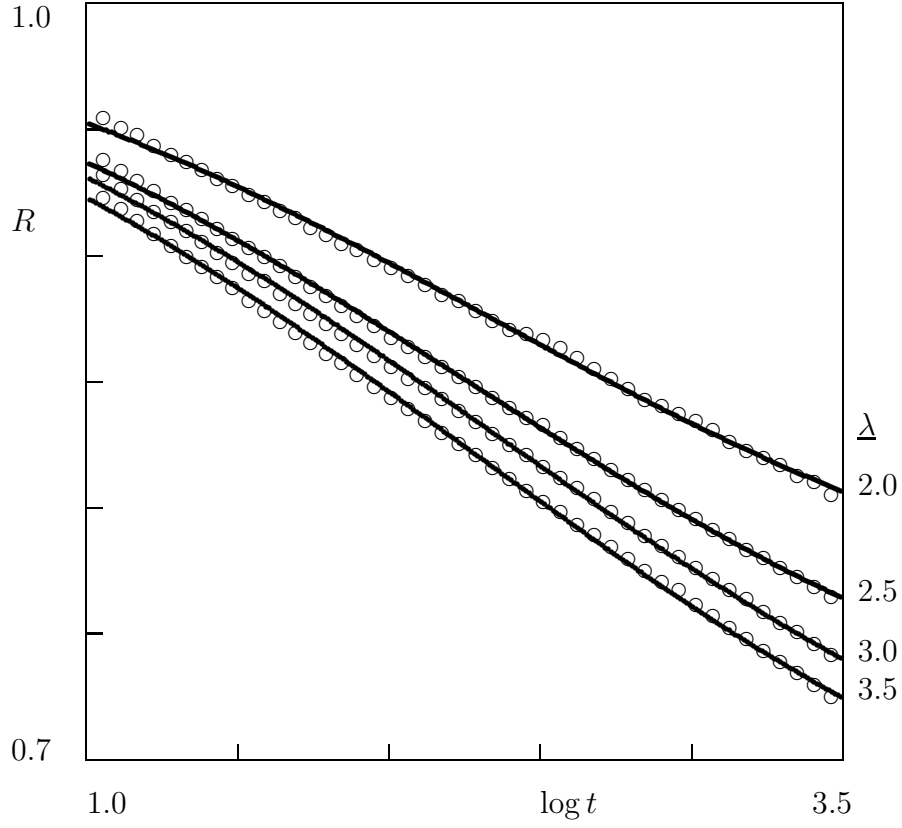


Figure 1: The dimensionless ratio R versus time t s in a relaxation test with the elongation ratio λ (virgin specimens). Circles: experimental data. Solid lines: results of numerical simulation

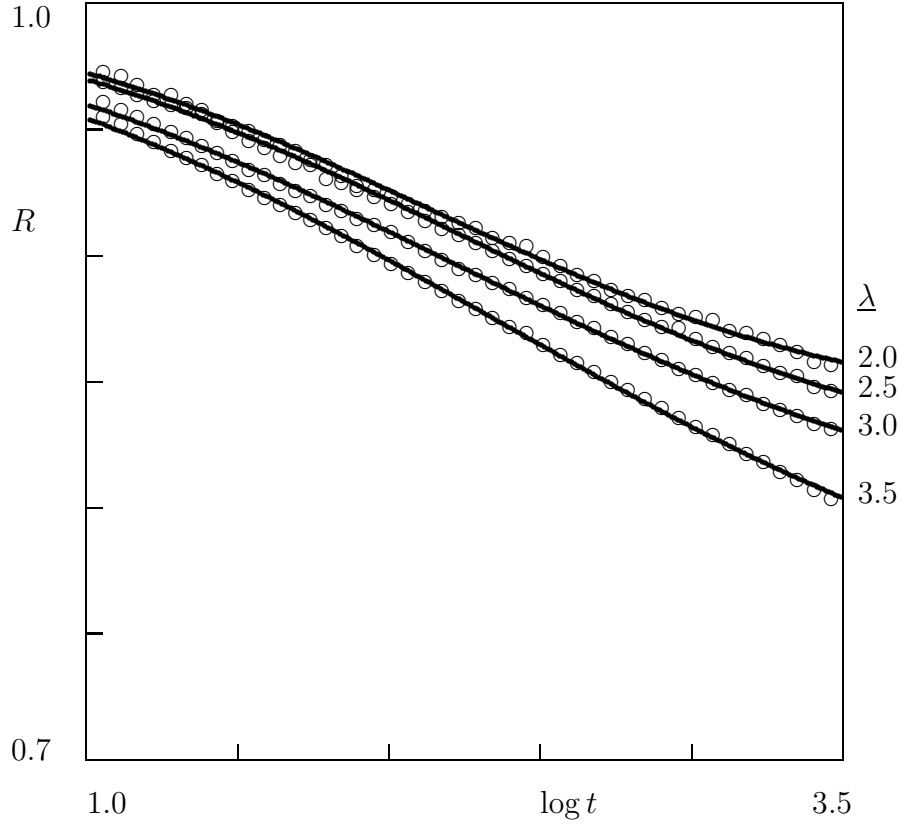


Figure 2: The dimensionless ratio R versus time t s in a relaxation test with the elongation ratio λ (the specimens after pre-loading). Circles: experimental data. Solid lines: results of numerical simulation

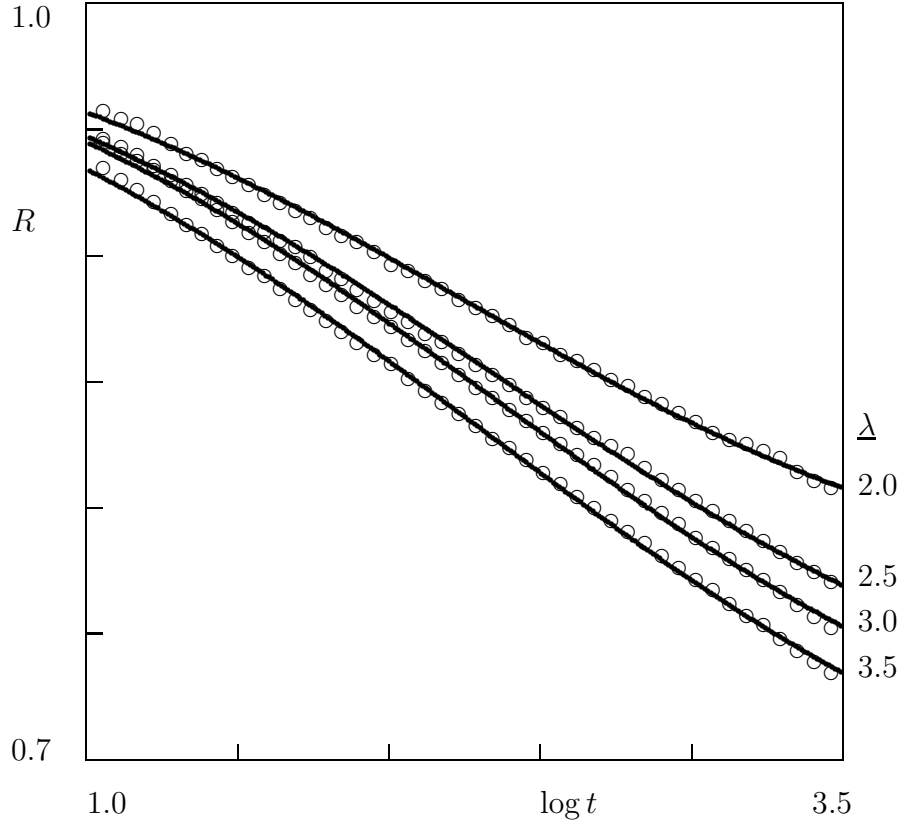


Figure 3: The dimensionless ratio R versus time t s in a relaxation test with the elongation ratio λ (the specimens after recovery). Circles: experimental data. Solid lines: results of numerical simulation

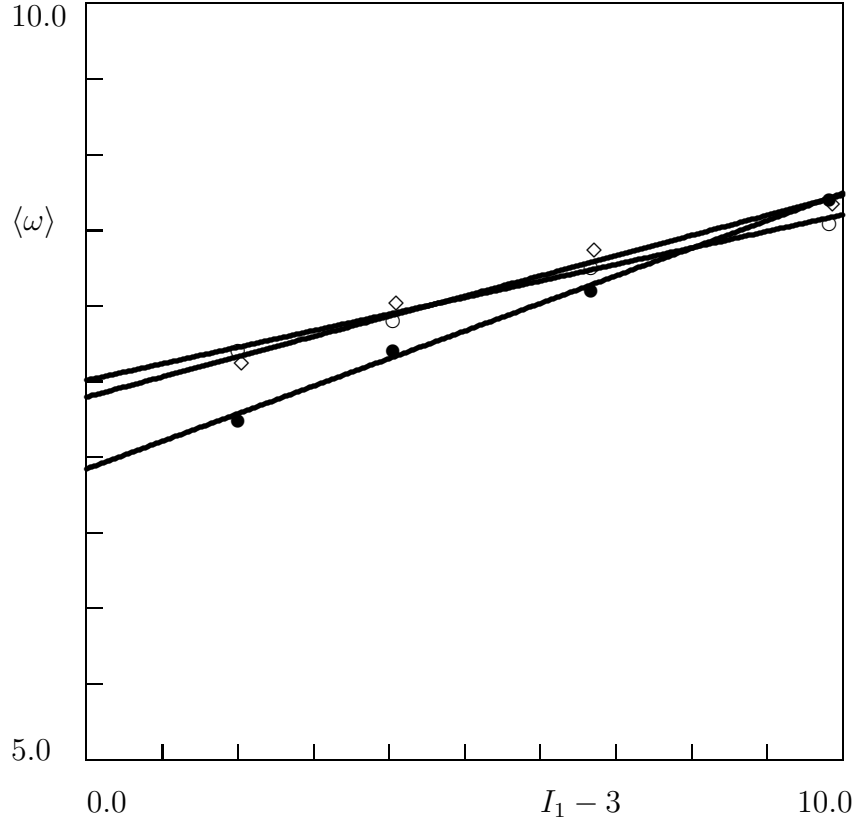


Figure 4: The average potential energy for sliding of junctions $\langle \omega \rangle$ versus the first invariant I_1 of the Cauchy deformation tensor. Symbols: treatment of observations. Unfilled circles: virgin specimens; filled circles: the specimens after pre-loading; diamonds: the specimens after recovery. Solid lines: approximation of the experimental data by Eq. (76)

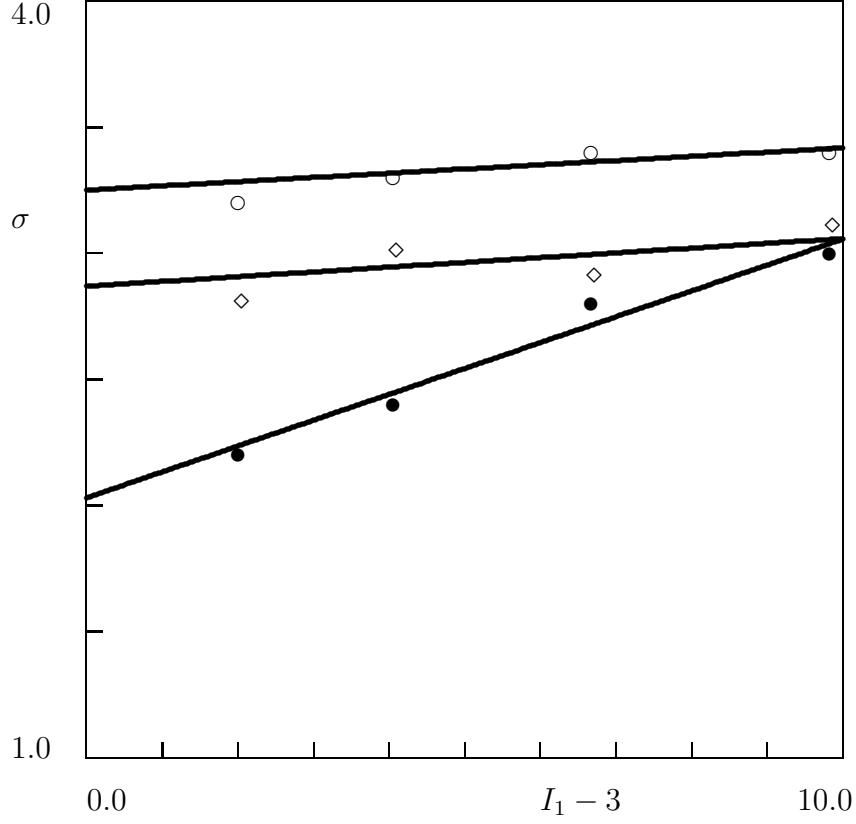


Figure 5: The standard deviation of potential energies σ versus the first invariant I_1 of the Cauchy deformation tensor. Symbols: treatment of observations. Unfilled circles: virgin specimens; filled circles: the specimens after pre-loading; diamonds: the specimens after recovery. Solid lines: approximation of the experimental data by Eq. (76)

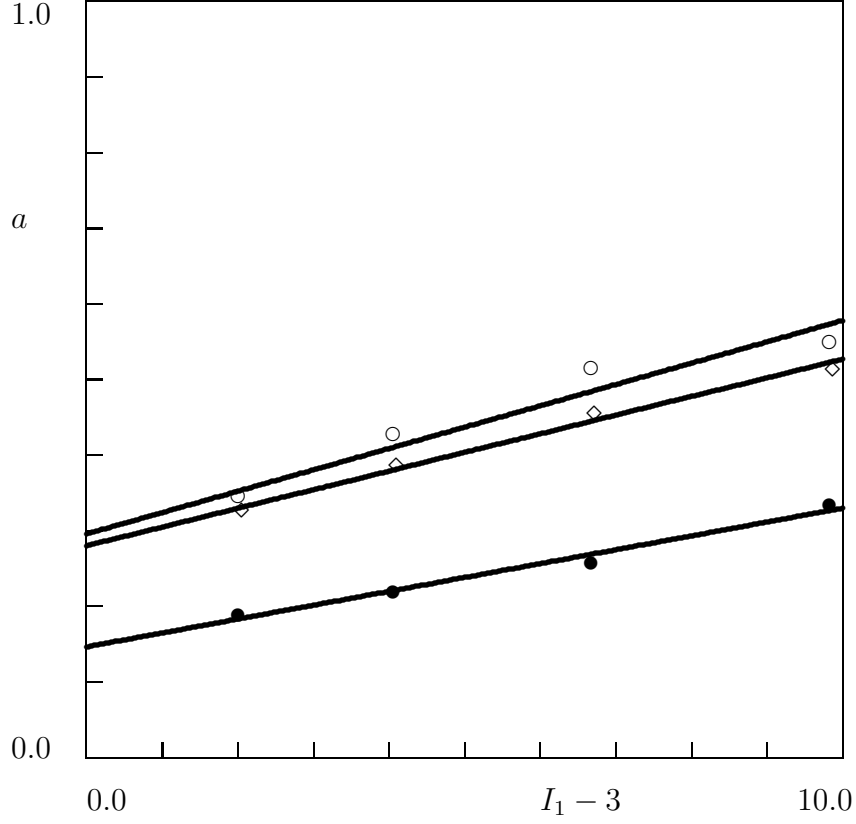


Figure 6: The dimensionless parameter a versus the first invariant I_1 of the Cauchy deformation tensor. Symbols: treatment of observations. Unfilled circles: virgin specimens; filled circles: the specimens after pre-loading; diamonds: the specimens after recovery. Solid lines: approximation of the experimental data by Eq. (79)

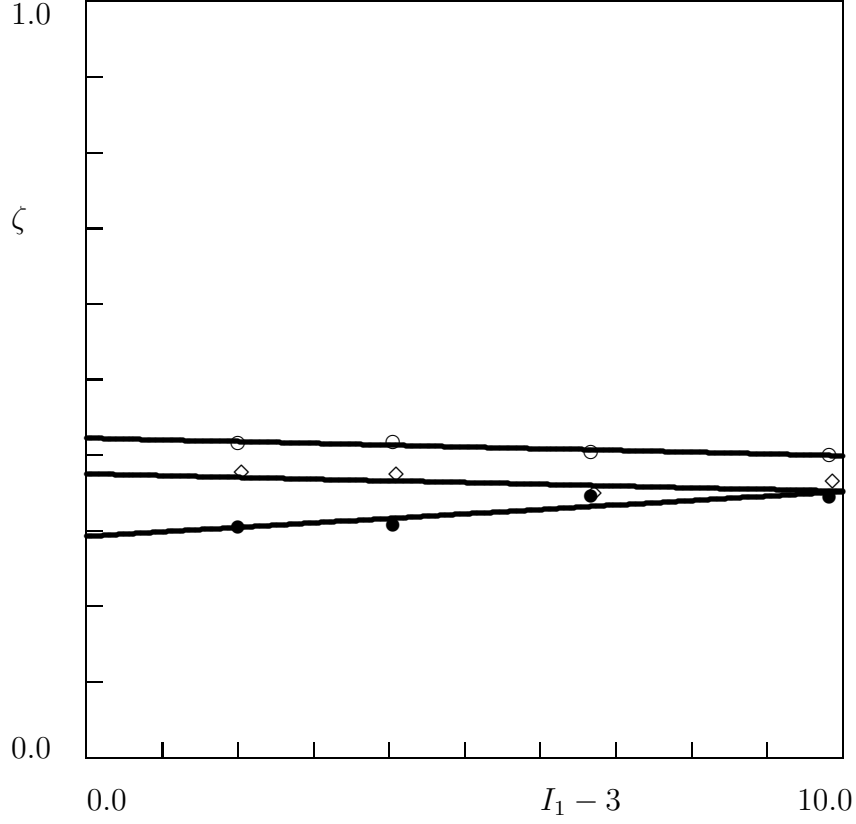


Figure 7: The dimensionless parameter ζ versus the first invariant I_1 of the Cauchy deformation tensor. Symbols: treatment of observations. Unfilled circles: virgin specimens; filled circles: the specimens after pre-loading; diamonds: the specimens after recovery. Solid lines: approximation of the experimental data by Eq. (80)